BILINGUAL PUBLISHING GROUP

**Journal of Environmental & Earth Sciences**

https://journals.bilpubgroup.com/index.php/jees

**ARTICLE**

# Time-Lapse Geoenvironmental Hydrocarbon Attenuation in Nigeria: Integrated Geoelectrical, Geochemical and Geotechnical Site Characterization

***Nurudeen Ahmed Onomhoale*** [1] **, *Nik Norsyahariati Nik Daud*** [1*] **, *Ipoola Ajani Okunlola*** [2] **, *Syazwani Idrus*** [1] **, *Siti Nur Aliaa Roslan*** [1]

[1] *Department of Civil Engineering, Faculty of Engineering, Universiti Putra Malaysia, Serdang 43400, Malaysia*

[2] *Chemical and Geological Sciences Department, Al-Hikmah University, Ilorin 240281, Nigeria*

## ABSTRACT

Hydrocarbon contamination from oil spills presents geoenvironmental and geoengineering challenges, notably in Eleme, Nigeria. This study integrates electrical resistivity tomography (ERT), soil total petroleum hydrocarbon (TPH) analysis, and geotechnical testing for treated spill site monitoring and characterization over six months. Four 100 m ERT lines, L1 to L4, with spacings at 1.5 m, 3 m, 6 m, 9 m, 12 m, and 15 m, were established for the first and second sampling phases. Twenty-one soil samples, 12 TPH, and 9 mechanical analyses, were obtained from 5 boreholes, BH1 to BH4, for the study site and the BH5 control site across the phases at 0.5 m, 3.0 m, and 5.0 m depths along ERT lines. ERT results reveal resistivity reductions averaging 18% in shallow zones of active degradation, correlating with an average 41% TPH-decrease. Specific gravity averaged 2.49 in the spill soils, compared to 2.58 in control samples, reflecting hydrocarbon-induced density reductions of 3.5%. Particle size showed spill soils contained > 50% fines, increasing water retention and reducing permeability by 30%. Consolidation tests highlighted increased compressibility, with settlements of 1.89 mm in spill soils versus 1.01 mm in control samples, indicating a 47% increase in settlement from hydrocarbon reduction. Correlation analysis shows slower consolidation at BH3 (−0.62 Cv) with moderate settlement increase (0.25), while BH4 exhibits

*CORRESPONDING AUTHOR:

Nik Norsyahariati Nik Daud, Department of Civil Engineering, Faculty of Engineering, Universiti Putra Malaysia, Serdang 43400, Malaysia; Email: niknor@upm.edu.my

ARTICLE INFO

Received: 14 July 2025 | Revised: 7 August 2025 | Accepted: 13 August 2025 | Published Online: 31 August 2025

DOI: https://doi.org/10.30564/jees.v7i8.11042

CITATION

Onomhoale, N.A., Daud, N.N.N., Okunlola, I.A., et al., 2025. Time-Lapse Geoenvironmental Hydrocarbon Attenuation in Nigeria: Integrated Geoelectrical, Geochemical and Geotechnical Site Characterization. Journal of Environmental & Earth Sciences. 7(8): 408–436. DOI: https://doi.org/10.30564/jees.v7i8.11042

much higher compressibility (0.95) but minimal Cv impact (0.23), indicating increased structural weakness with higher residual TPH. Spill degradation reduced TPH by 19%–64% in shallow zones, with persistent contamination at deeper layers exceeding the regulatory limits, emphasising the need for ongoing monitoring and targeted remediation for long-term stability and sustainability.

***Keywords:*** Degradation Monitoring; Geoenvironmental Hydrocarbon Contamination; Time-Lapse Electrical Resistivity Tomography (TL-ERT); Soil Mechanical Properties; Temporal Geochemical Assessment; Correlation Matrix

# 1. Introduction

Oil spills in Nigeria have become a critical environmental issue, particularly in the Niger Delta, an area that has seen extensive oil exploration and production activities for decades [1]. The accidental release of hydrocarbons into the environment, a frequent occurrence due to operational failures and infrastructure decay, poses severe threats to terrestrial and aquatic ecosystems [2]. These spills contaminate soil and water bodies, adversely affecting biodiversity, agriculture, and the health of local communities [3]. The complexity and persistence of hydrocarbon pollutants in the environment necessitate complementary approaches for monitoring and evaluating the clean-up and attenuation strategies [4]. While it is functional, employing only the traditional soil chemical analyses does not provide a comprehensive view of contaminant degradation's spatial and temporal dynamics and soil recovery [5]. This gap in monitoring technology has led to the exploration of integrated approaches that employ geoelectrical, geochemical, and geotechnical techniques [6].

Electrical resistivity tomography (ERT) is a potent geophysical tool for observing subsurface changes without disrupting the soil matrix, making it ideal for longitudinal studies [2,7]. It offers the unique advantage of visualizing the degradation of hydrocarbons in situ, providing a temporal and spatial understanding of the contaminant reduction [8]. Hydrocarbons degrade, producing byproducts such as water, carbon dioxide, and various organic acids [9]. These byproducts can alter the electrical properties of the soil, typically resulting in increased soil moisture and the release of ions that affect soil conductivity [3]. Over time, as hydrocarbon breakdown progresses, these changes are reflected in ERT surveys as variations in resistivity values. A decrease in hydrocarbon concentration generally corresponds to a reduction in resistivity, indicating practical spill degradation [10]. Concurrently, TPH analysis is employed to quantify the actual hydrocarbon content in soil samples, offering precise chemical data on the levels of aliphatic hydrocarbons present [7]. Integrating TPH data with ERT results provides a comprehensive understanding of how degradation dynamics influence subsurface resistivity [9]. By comparing resistivity values at different time intervals, this study can assess the rate of spill degradation and the corresponding reduction in hydrocarbon contaminants [3].

It is of paramount importance to assess the reduction in hydrocarbon mass over time and to understand how these changes affect the soil's chemical, physical and mechanical properties [11], influencing and controlling geoenvironmental characteristics like the strength of the soil fabric and its ability to resist particle detachment during erosion [12], and geotechnical characteristics such as natural moisture content, specific gravity, particle size distribution, atterberg limits, shear strength, and consolidation characteristics [13]. Evaluating the consequential effects of hydrocarbon degradation on these characteristics provides critical information concerning the environmental and engineering profiles of impacted areas [9]. The geoenvironmental includes details on the changes in soil stability, erosion potential, and overall soil health [11], while geotechnical profiling is critical as it influences the soil's behaviour under different conditions like mechanical stress and its ability to support structural [12], which are key considerations in the recovery and future use of remediated lands [8]. Understanding these impacts is essential for developing sustainable land management practices and preventing further environmental degradation [3,13].

The impact of TPH on these soil properties and characteristics is highly significant and multifaceted [9]. Hydrocarbon contamination can alter the soil's moisture content by either repelling water due to the hydrophobic properties of oil or trapping water within the soil matrix, leading to changes in soil consistency and workability [12]. Hydrocarbons can lower the specific gravity of soil particles, as hydrocarbons

are generally less dense than soil minerals [14]. This alteration affects the overall density and stability of the soil. Additionally, hydrocarbon contamination can cause aggregation of soil particles, leading to changes in soil texture and particle size distribution [13]. This affects the soil's permeability and capacity to support microbial activity essential for degradation [15]. Furthermore, contaminated soils often exhibit altered plastic and liquid limits [15]. Hydrocarbons can reduce the soil's plasticity, making it less pliable and affecting its structural integrity. The shear strength of soil can be significantly reduced by the presence of hydrocarbons, as the lubricating effect of oil reduces interparticle friction [9]. This reduction in shear strength compromises the soil's ability to support loads. Hydrocarbons can also affect the compressibility of soils [12]. Contaminated soils may exhibit increased consolidation rates and altered settlement behaviour, impacting the stability of structures built on such soils [6].

Altered moisture content and specific gravity can reduce soil fertility, affecting plant growth and agricultural productivity [12]. Changes in soil texture and permeability can result in poor drainage, leading to waterlogging or increased runoff, which can cause erosion and further spread contaminants [11]. Reduced plasticity and shear strength can compromise soil stability, increasing the risk of subsidence, which can threaten infrastructure and human safety [7]. Increased consolidation rates and altered settlement behaviour can affect the structural integrity of buildings and other constructions, leading to potential hazards [12]. By integrating temporal geoelectrical and geochemical data with traditional geotechnical testing, this study aims to provide a more dynamic and detailed analysis of contaminants mass reduction [5] and current site-specific conditions of previously cleaned-up efforts of contaminated areas in Nigeria [16].

This research endeavours to contribute valuable insights into the adaptive management of soil restoration practices, aiming for environmental sustainability in oil-impacted regions [3]. It also seeks to establish a model for similar environmental and engineering monitoring efforts in other areas facing comparable challenges [13]. This study introduces an integrated approach to environmental and engineering monitoring of spill sites by utilizing time-lapse electrical resistivity tomography (TL-ERT) and temporal geochemical assessment using soil total petroleum hydrocarbon (TPH) analyses [17,18]. Major spills in Nigeria occurred in the Niger Delta region [3,16,18], and national clean-up efforts commenced in 2018 [12,19]. These efforts are executed by the Federal Ministry of Environment, Hydrocarbon Pollution Remediation Project [19], following the United Nations Environment Programme [20] environmental assessment report [21,22]. HYPREP largely employs the ex-situ treatment process, particularly biostimulation for contaminated land clean-up involving soil treatments in a biopile by nutrient addition [7,19,23]. Biostimulation enhances the natural biodegradation process by supplying essential nutrients that stimulate the growth and activity of indigenous hydrocarbon-degrading microorganisms [12]. Nutrient additions like urea and Nitrogen, Phosphorus, and Potassium (NPK) at specific ratios have been shown to significantly accelerate the breakdown of hydrocarbons, thereby reducing contamination levels more rapidly than natural attenuation processes alone [15]. This treatment not only aids in the degradation of hydrocarbons but also improves soil fertility and promotes ecosystem recovery [3].

The findings of this research are expected to demonstrate the degradation dynamics and attenuation rate of contaminants in improving soil quality [13]. ERT and TPH analyses provide a comprehensive monitoring framework that captures the chemical and physical changes in the soil during the hydrocarbon-mass reduction process [24]. The anticipated reduction in resistivity values over time, correlated with decreasing TPH levels, will offer robust evidence of the effectiveness of nutrient-enhanced biodegradation [10]. Understanding the impacts of hydrocarbon degradation on geotechnical and geoenvironmental characteristics is crucial for assessing the long-term viability of treated soils for agricultural or construction purposes [24]. Improved soil moisture content, specific gravity, particle size distribution, atterberg limits, shear strength, and consolidation characteristics post-treatment will indicate progressive attenuation for better soil health and functionality [13]. In conclusion, this study aims to bridge the gap in current monitoring techniques of contaminants attenuation in hydrocarbon sites in Eleme, Rivers State, Nigeria, by providing a holistic approach that incorporates geoelectrical, geochemical, and geotechnical methods, focusing on TL-ERT survey, soil TPH analysis, specific gravity, particle size distribution, and consolidation. The insights gained from this research will inform better monitoring and evaluation practices in Nigeria and contribute to global

knowledge on effective management of oil-contaminated environments.

## 2. Study Location and Geology

Rivers State, located in the Niger Delta region of southern Nigeria, lies at latitude 4.8396° N and longitude 6.9112° E (**Figure 1**). The state is bordered to the north by Imo and Anambra, to the east by Abia and Akwa Ibom, and to the west by Bayelsa and Delta. Port Harcourt, the state capital, is a central commercial hub for Nigeria's oil industry[25]. The study location, Eleme, is a local government area within Rivers State, situated at longitude 4.7843° N and latitude 7.1393° E. Eleme shares borders with Okrika and Ogu/Bolo LGAs to the south, Tai LGA to the east, and Port Harcourt City, Obio/Akpor, and Oyigbo LGAs to the west[26]. Industrialization and economic opportunities have driven rapid urbanization and population growth in Eleme, increasing immigration[7]. The area spans approximately 230 square kilometres, with the Eleme people as the predominant ethnic group. Its towns and communities include Ogale, Nchia, Akpajo, Alode, Ebubu, Onne, Eteo, Alesa, and Aleto[27]. Eleme, located at the western end of Ogoniland, is divided into two administrative units: the Nchia bloc, comprising six clans (Akpajo, Aleto, Alesa, Alode, Ogale, and Agbonchia), and the Odido bloc, which includes four clans (Onne, Ebubu, Eteo, and Ekporo); each clan contains numerous sub-communities[7].

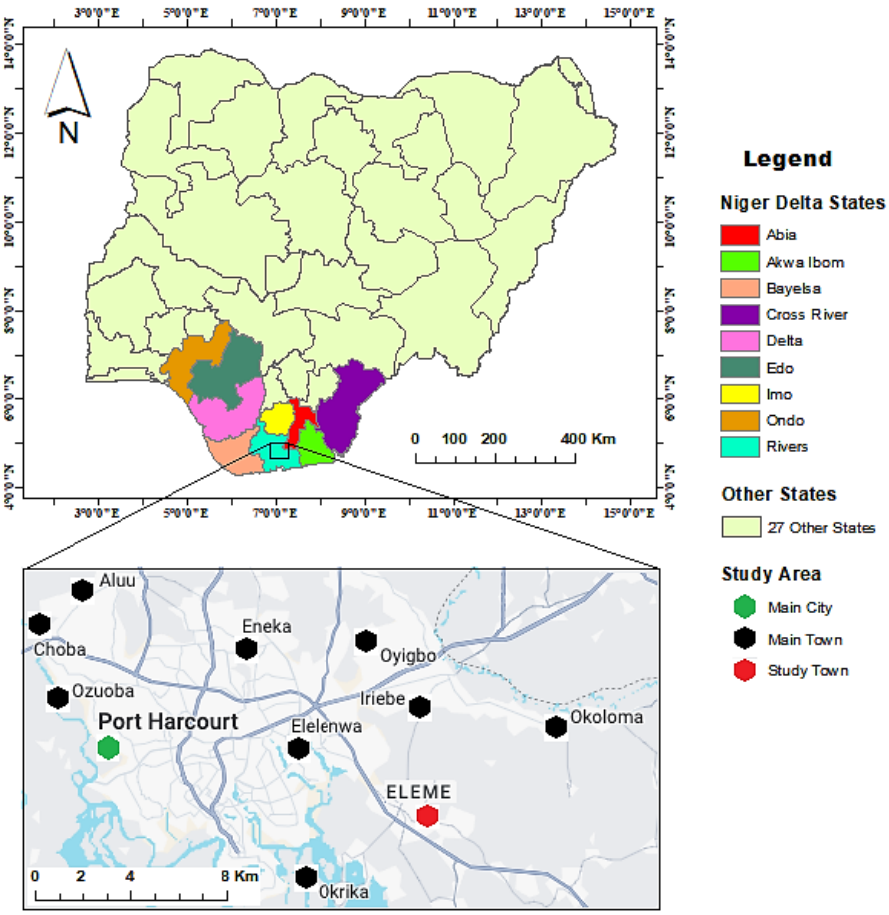


**Figure 1.** Map showing Nigeria and the Niger Delta with highlight of study area in rivers state.

Source: Author.

The study area is primarily accessible via the Port Harcourt–Uyo Expressway, which connects to the East-West Road. Historically, agriculture has been the predominant occupation in Eleme, with farming forming the backbone of livelihoods in the area[26]. The primary crops cultivated in the area include yams, cocoyams, cassava, sugar cane,

and pumpkins, among others, emphasizing the necessity for healthy and uncontaminated soils to mitigate risks of food-borne diseases[26]. Farmlands are generally structured into large communal blocks, with individual families owning delineated portions for cultivation[27]. Geologically, Eleme lies within the Niger Delta Basin, which was formed during the Tertiary period through repeated cycles of subsidence and sediment deposition caused by oceanic activities[28]. This geological evolution led to three central litho-stratigraphic units: the Akata, Agbada, and Benin formations[29,30]. The Benin formation, which underpins this study, is particularly significant among these. The Eleme area is underlain by the Sombreiro-Warri Deltaic Plain sands, dating from the Quaternary to Recent periods[30]. These sands are typified by sandy silt, brownish lateritic soils (clayey/silty sand), and fine to medium/coarse-grained unconsolidated sands[31]. Notably, the Benin formation is a significant aquifer critical to the area's groundwater resources[30].

# 3. Material and Methods

## 3.1. Fieldwork, Sampling and Data Acquisition

The study systematically investigated the attenuation site over two sampling phases spaced 185 days (roughly six months) apart. This was established to monitor and evaluate changes in soil conditions, maintaining consistent survey lines and sampling points for accurate analysis[32]. The survey site location, coordinates, and survey line geometry, along with data specifics, are summarized in **Table 1**, while the sample stations, borehole points coordinates, and identification are presented in **Table 2**. Survey lines and sampling grids were carefully documented, and data acquisition adhered to standard field protocols. Due to site constraints, including the proximity of a highway, the survey lines and sampling points were oriented from southwest to northeast and aligned parallel to the pipeline, as depicted in the Google Earth imagery shown in **Figure 2**.

**Table 1.** Description and identification of geoelectrical survey lines and periods.

| **Survey Period** | | **First Phase** | | **Second Phase** | |
|---|---|---|---|---|---|
| Line No. | | Line 1 (L1) | Line 2 (L2) | Line 3 (L3) | Line 4 (L4) |
| Line Length (m) | | 100 | 100 | 100 | 100 |
| Line Orientation | | NE-SW | NE-SW | NE-SW | NE-SW |
| Line Start (LS) | N | 4.771742 | 4.771900 | 4.771747 | 4.771892 |
| Coordinates | E | 7.126450 | 7.126342 | 7.126464 | 7.126361 |
| Line End (LE) | N | 4.772181 | 4.772364 | 4.772200 | 4.772383 |
| Coordinates | E | 7.127256 | 7.127167 | 7.127269 | 7.127183 |
| Zone | | 32 N | 32 N | 32 N | 32 N |

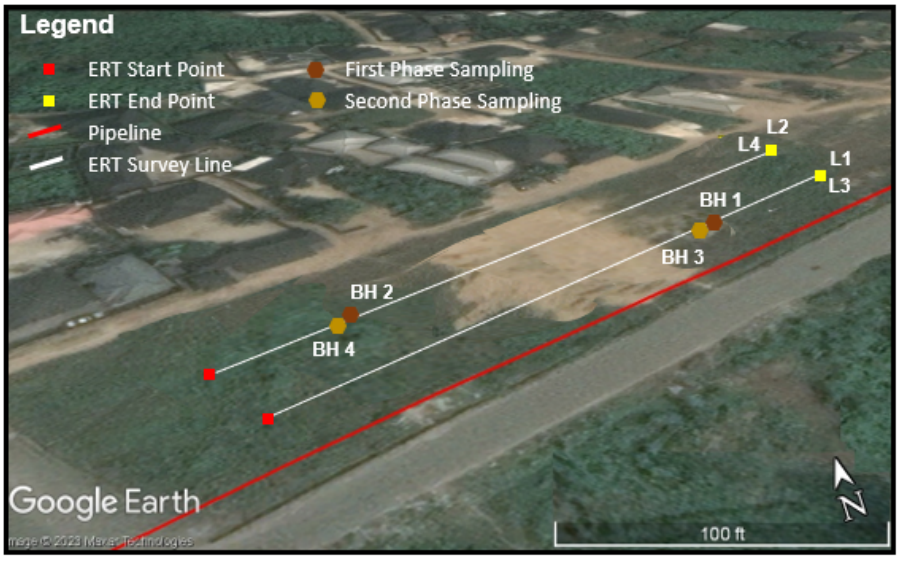


**Figure 2.** Map showing the study site, survey lines and sampling stations.

Source: Author.

**Table 2.** Description and identification of samples.

| Sample | | | | | | Coordinates | |
|---|---|---|---|---|---|---|---|
| **S/No.** | **Stations** | **Reference** | **Depth (m)** | **Sampling** | **Analysis** | **Latitude (N)** | **Longitude (E)** |
| SN 1 | SC-1 | BH 1 | 0.5 | First Phase | Chemical | 4.77212222 | 7.12711389 |
| SN 2 | SC-2 | | 3.0 | | | 4.77212222 | 7.12711389 |
| SN 3 | SC-3 | | 5.0 | | | 4.77212222 | 7.12711389 |
| SN 4 | SC-4 | BH 2 | 0.5 | | | 4.77200833 | 7.12650833 |
| SN 5 | SC-5 | | 3.0 | | | 4.77200833 | 7.12650833 |
| SN 6 | SC-6 | | 5.0 | | | 4.77200833 | 7.12650833 |
| SN 7 | SC-7 | BH 3 | 0.5 | Second Phase | | 4.77211389 | 7.12710833 |
| SN 8 | SC-8 | | 3.0 | | | 4.77211389 | 7.12710833 |
| SN 9 | SC-9 | | 5.0 | | | 4.77211389 | 7.12710833 |
| SN 10 | SC-10 | BH 4 | 0.5 | | | 4.77201389 | 7.12650278 |
| SN 11 | SC-11 | | 3.0 | | | 4.77201389 | 7.12650278 |
| SN 12 | SC-12 | | 5.0 | | | 4.77201389 | 7.12650278 |
| SN 13 | SM-1 | BH 3 | 0.5 | Second Phase | Mechanical | 4.77211389 | 7.12710833 |
| SN 14 | SM-2 | | 3.0 | | | 4.77211389 | 7.12710833 |
| SN 15 | SM-3 | | 5.0 | | | 4.77211389 | 7.12710833 |
| SN 16 | SM-4 | BH 4 | 0.5 | | | 4.77201389 | 7.12650278 |
| SN 17 | SM-5 | | 3.0 | | | 4.77201389 | 7.12650278 |
| SN 18 | SM-6 | | 5.0 | | | 4.77201389 | 7.12650278 |
| SN 19 | CT-1 | BH 5 | 0.5 | Control | | 4.77588333 | 7.12758333 |
| SN 20 | CT-2 | | 3.0 | | | 4.77588333 | 7.12758333 |
| SN 21 | CT-3 | | 5.0 | | | 4.77588333 | 7.12758333 |

The geophysical survey employed a grid pattern using four electrical resistivity tomography (ERT) lines configured with a four-electrode Wenner array [33]. Each line measured 100 meters long, with electrode spacings of 1.5 m, 3 m, 6 m, 9 m, 12 m, and 15 m, following established guidelines by Ahmed et al. [7]. The lines established in each survey phase facilitate a detailed site investigation consisting of L1 and L2 for the first phase and L3 and L4 for the second phase. Their orientations and configurations were explicitly chosen to accommodate the physical layout and constraints of the site while ensuring comprehensive coverage for monitoring and data acquisition [7]. The study site's geochemical (soil chemical) and geotechnical (soil mechanical) evaluations were conducted using 18 subsurface soils collected across the two investigation phases. Each phase included six samples obtained from 4 boreholes, consisting of BH1 and BH2 for the first phase sampling and BH3 and BH4 for the second phase sampling, at depths of 0.5 m (top), 3 m (middle), and 5 m (bottom) to assess vertical variations in soil properties [34]. Relatively consistent borehole positions were maintained throughout the study to enable reliable comparisons of results over the study interval [32]. The sampling scheme also included 3 (three) additional control samples (CT1, CT2, and CT3) obtained from uncontaminated sites (BH5) to compare geotechnical properties [24].

The samples were collected using hand augers and transported to the laboratory for detailed geotechnical and geochemical analysis. The boreholes where the soil samples were obtained were strategically located around the 25 m and 75 m horizontal ground distances along the ERT lines, with BH1 and BH3 situated around the 25 m mark of L1 and L3, while BH2 and BH4 were located around the 75 m mark of L2 and L4. Surveys and sampling were conducted within two days after backfilling the ex-situ treated soils and repeated approximately six months later to evaluate the progression of site characteristics and recovery dynamics [2]. Systematic random sampling achieved even spatial distribution, with precise coordinates and sampling station recording, ensuring a representative study area analysis [32]. To preserve sample integrity, collected soil samples were placed in airtight plastic bags and stored in ice-packed coolers, shielded from direct sunlight [35]. The samples were then transported promptly to the laboratory for comprehensive analysis. This approach minimized contamination and degradation, ensuring high-quality data for evaluating the recovery of the site [7]. This combined survey and sampling approach ensured that the vertical profile, horizontal representation, and spatiotemporal changes in the soil's physical, chemical, and mechanical characteristics were adequately captured for meaningful evaluation [36].

## 3.2. Geoelectrical Soil Analysis

The tools and equipment used for electrical resistivity tomography (ERT) investigations included a PASI 16GL digital earth resistivity meter, four metal electrodes, four reels of cable, two hammers, 100-meter measuring tape, Garmin GPS devices, 12-volt batteries, pre-prepared data sheets, and a digital camera. These materials were arranged and utilized on-site based on the selected survey method and field design. A base map of the study site guided the planning of survey line paths and trajectories. **Figure 3a** illustrates the field instrumentation, with each survey line spaced 5 m apart and aligned parallel to the sabotaged pipeline. The Wenner array was selected due to its ability to capture depth effectively, lateral extent, and plume migration pathways [37,38]. Smaller electrode spacing was used to obtain high-resolution 2D ERT data for near-surface contamination impacts without excluding crucial information [33]. ERT measurements require numerous four-electrode resistivity readings to create 2D models of the subsurface. Using surface or borehole electrodes, these measurements map resistivity variations to depict subsurface conditions [37]. The Wenner array configuration utilized current electrodes (C1 and C2) to inject electrical current and potential electrodes (P1 and P2) to measure voltage differences, following Ohm's Law [37,38]. Apparent resistivity (ρa) values were calculated by multiplying resistance (R) by the geometric factor ($K = 2\pi a$) [33]. Given a water table depth of approximately 6.5 m, target exploration depths minimally exceeded this limit. The data collected were processed for analysis after being converted to apparent resistivity values. Acquired field data were processed using Earth Imager 2D software [7], while the survey maps and data points were digitized using ArcGIS and Google Earth [39].

The ERT data processing applied a finite difference and least-squares approach to reconstruct geological models from apparent resistivity data [37,40]. Inversion algorithms used relied on a smoothness-constrained least-squares method. Adjustable damping factors and roughness filters refined the models for site-specific conditions [41]. The inversion achieved satisfactory results for this study within four iterations, with root-mean-square (RMS) errors consistently below 10% [40]. Topographic variations were negligible, eliminating the need for elevation data during inversion. **Table 3** provides resistivity values for common rocks and soils, aiding material delineation and subsurface characterization [42]. Resistivity contrasts depend on the spill's age [8]; recent oil spills create elevated resistivity anomalies, while older or treated spills exhibit subtler contrasts due to physical, chemical, and biological alterations [43,44]. Fresh hydrocarbon spills impede electrical current flow by displacing conductive soil pore water [12]. This research focuses on mature and treated soils, leveraging anticipated resistivity anomalies to identify hydrocarbon contamination behaviours in geologic materials [45]. The results emphasize the necessity of high-resolution data and comprehensive analysis for effective environmental and subsurface investigations, ensuring the accurate identification of contaminant degradation, monitoring, and attenuation dynamics.

**Table 3.** Resistivity values of common rocks and soil materials [42].

| Material | Resistivity (Ωm) |
|---|---|
| Alluvium | 10 to 800 |
| Sand | 60 to 1000 |
| Clay | 1 to 100 |
| Laterite Soil | 120–750 |
| Sandy Clay / Clayey Sand | 30–215 |
| Sandstone | 8–4000 |
| Shale | 20–2000 |
| Limestone | 50–4000 |
| Gravel and Sand | 500–5000 |

## 3.3. Geochemical Soil Analysis

TPH concentrations were assessed to determine the sample's petroleum aliphatic hydrocarbon levels, C6 to C40. This analysis utilized a Gas Chromatograph fitted with a Flame Ionization Detector (GC-FID) [46]. Specifically, the study employed an Agilent 7820A Gas Chromatograph equipped with an HP-5 fused silica capillary column measuring 30 m × 0.32 mm ID × 0.25 μm film thickness [46]. Helium was used as the carrier gas at a flow rate of 1.75 mL/min, with an average velocity of 29.47 cm/sec, and a precisely measured 1 μL aliquot of purified sample extract was injected in splitless mode at an injection temperature of 300 °C [47]. The column temperature was programmed to begin at 40 °C, where it was held for one minute, then increased at a rate of 7 °C per minute until reaching a final temperature of 320 °C [48]. The detector temperature was maintained at 300 °C throughout the analysis. These procedures align with the methodologies described by Inyang et al. [47] and Kim et al. [48].

The gas chromatograph was calibrated using petroleum hydrocarbon calibration standards prepared within a 0.05–20 μg/mL range, using n-hexane as the diluent [46]. Calibra-

tion curves were constructed, and average response factors for each analyte were generated using Agilent Chemstation software[46]. The calibration curves demonstrated linearity, with correlation coefficients ranging from 0.9846 to 0.9919. To quantify unresolved peaks, the response factor of nC-15 was applied, following the approach outlined by Luan and Szelewski[46]. The TPH content in the samples was determined by integrating the baseline-holding peaks and summing the concentrations of n-alkanes eluting between nC-9 and nC-36, along with the unresolved complex mixtures (UCM)[48]. The ratios of low molecular weight n-alkanes to high molecular weight n-alkanes and unresolved n-alkanes to resolved n-alkanes were calculated using Agilent software. This approach was consistent with the methodologies elaborated by Luan and Szelewski[46]. The collected samples using hand augers (**Figure 3b**) from different borehole stations, depths, and sampling phases with the soil TPH analysis for each of the samples were compared with established standards of the Department of Petroleum Resources (DPR)–Environmental Guidelines and Standards for the Petroleum Industry in Nigeria[49] for TPH contamination levels and soil quality assessment.


**Figure 3.** (**a**) ERT survey investigation; (**b**) auger borehole soil sampling.

## 3.4. Geotechnical Soil Analysis

The soil samples underwent air-drying and were tested to determine key geotechnical index properties[35], including Specific Gravity, Particle Size Distribution, and Consolidation behaviours[50]. Since the study emphasizes attenuation monitoring for site characterization, the utilized geotechnical tests focused on the soil's compositional and compressive properties[51], which are essential for understanding geochemical changes in response to hydrocarbon degradation[13,50]; hence, the choice of the three geotechnical soil analysis. Specific gravity (Gs) provides insight into the density changes in soil particles as hydrocarbon degradation progresses, affecting geotechnical behaviour[24]. Particle size distribution is essential for tracking changes in soil texture and composition, which may be influenced by biodegradation and affect porosity and permeability[12]. Consolidation helps analyze long-term settlement properties in response to biodegradation and is crucial for understanding soil compressibility in post-spill scenarios[50]. These tests are selected for their relevance to compositional changes, density, and long-term stability under biodegradation[29], aligning with the study's focus on temporal geoelectrical and geochemical monitoring[24].

Specific gravity (Gs) is the ratio of the mass of dry soil in the air to the mass of an equal volume of distilled water at 20 °C, which is essential for understanding soil properties[35]. A pycnometer, a 0.9-liter density bottle, is used for this test. The pycnometer is cleaned and weighed empty, then filled with approximately 200 g of oven-dried soil, and weighed again after being filled with water[50]. Finally, the pycnometer is filled with water only, and its weight is recorded. These measurements allow for the accurate calculation of specific gravity, which is crucial for analyzing soil behaviour in engineering and environmental applications[52]. Particle size distribution analysis determines grain size and sorting characteristics of soil[52]. Using materials such as a British standard sieve and heavy-duty balance, soil samples are oven-dried, weighed (500 g), and soaked in water for 24 hours to disaggregate particles[50]. The sample is washed over a 20 mm sieve, oven-dried again, and weighed

to determine the weight of fine particles removed. The dried sample is sieved, and the weight of soil retained on each sieve is recorded[35]. Results provide insights into soil texture and its suitability for engineering and environmental applications[12]. The oedometer consolidation test measures soil compression due to water removal from voids under sustained load[50]. It involves applying incremental loads (e.g., 10–1000 kN/m²) to a soil sample, typically 60 mm in diameter, with a thickness at least ten times the maximum grain diameter[35]. Settlement readings are taken at frequent intervals until 90% consolidation is achieved, followed by occasional observations until compression stops. After the test, the soil is unloaded and swelled[50]. This test is vital for understanding soil compressibility under structural or foundation loads[51]. All samples (**Figure 3b**) and analyses strictly adhered to standardized procedures for testing soils in civil engineering applications, as per the guidelines outlined in the Unified Soil Classification System[35] and the American Association of State Highways and Transportation[53] soil classification methods.

# 4. Results and Discussion

## 4.1. Time-Lapse Electrical Resistivity Tomography (TL-ERT) Monitoring

The first phase of the monitoring survey and soil mapping was carried out immediately after the backfilling of the ex-situ treated soils. This was done to get the non-invasive real-time soil properties to estimate its overall characteristics in the pedo-environmental system[54]. Four ERT lines were established, featuring L1, L2, L3, and L4 to represent the site's coverage area over the two phases due to the homogeneity of the post-treated soils. The average resistivity values across the lines and phases are depicted in **Table 4**.

**Table 4.** Average resistivity values across lines and the phases.

| Electrode Spacing (m) | Average Apparent Resistivity (Ωm) | | | |
|---|---|---|---|---|
| | First Phase | | Second Phase | |
| | Line 1 (L1) | Line 2 (L2) | Line 3 (L3) | Line 4 (L4) |
| 1.5 | 112.6278 | 100.1628 | 116.4171 | 97.0478 |
| 3.0 | 106.0375 | 104.5981 | 114.2706 | 110.2106 |
| 6.0 | 139.0837 | 111.5625 | 138.0012 | 173.1450 |
| 9.0 | 207.1877 | 125.0522 | 210.3687 | 203.9455 |
| 12.0 | 314.1983 | 269.3483 | 321.6916 | 305.3850 |
| 15.0 | 450.1800 | 410.0060 | 480.8980 | 444.4080 |

In previous studies by Ahmed et al.[7] and Ovuru and Udom[55], resistivity values above 600 ohms.m indicate oil-contaminated intervals in the area. This value was realized after carefully analyzing the behaviour of the resistivity values around the oil spill site alongside the background resistivity signatures from the control site[7], indicating uncontaminated soils as a baseline for the delineation. The distinct resistivity values associated with different soil types play a crucial role in delineating subsurface layers and understanding the characteristics of the subsurface environment[56]. Sandy soils, characterized by larger particles and higher permeability, facilitate rapid infiltration and spread of oil[12]. In contrast, clayey soils with smaller particles and lower permeability impede oil infiltration, leading to a slower spread and confinement to the surface[51]. According to previous studies, the analysis of geoelectrical images from the study area presents the lithological descriptions revealing a predominant presence of clayish and sandy soils[7]. However, soil variations like sandy clays, clayey sands, lateritic sands, and fine / medium-grained sand also contribute to the lithology and subsurface pathways of contaminants[7].

The Earth Imager software processed the 2D inversion geoelectric images generated for the survey lines[57]. The delineation focuses on subsurface areas from ground to 6 m maximum depths, representing the region marked in Trapezium, indicating the zone of impacted soils, where blue depicts lower resistivity, primarily corresponding with clay and more significant active biodegrading hydrocarbon[7] (**Figure 4a**). The green represents relatively higher resistivity values corresponding with sand-clay or clayey-sand and a lesser degree of ongoing hydrocarbon attenuation (**Figure 4b**). The resistivity values for the first monitoring phase lines ranged from 69.26 ohms.m to 683.1 ohms.m from the ground surface to the maximum depth of investigation. L1 has resistivity

values lowest at 69.26 ohms.m and a peak value of 683.17 ohms.m, while L2 recorded the highest resistivity of 515.31 ohms.m, with a minimum value of 73.75 ohms.m. The second phase surveys generally experienced a relative reduction in resistivity values ranging from 89.11 ohms.m to 598.14 ohms.m for L3 and from 63.29 ohms.m to 508.49 ohms.m for L4 across the depth of investigation. The surveys aimed to evaluate the status of attenuation and the soil quality [7] within the designated target area, identified by a Trapezium marking the zone under active biodegradation and contaminant mass reduction over six-month the monitoring period.

The time-lapse geoelectrical monitoring showed that the first phase survey revealed a range of resistivity values that indicate a general decrease compared to established spill values in the study area, as recorded by Amadi [58], Ovuru and Udom [55], and validated by the work carried out by Ahmed et al. [7]. The geoelectric images primarily displayed green colours representing medium to low resistivity in the treated areas. This suggests a significant reduction in hydrocarbon contamination following the initial sampling [59]. Line 2 exhibited the most substantial drop in resistivity, suggesting more active biodegradation in this area. In contrast, Line 1 displayed progressively lesser reduction in resistivity, implying varying levels of degradation effectiveness across the site [24]. For L3 and L4, although the resistivity values were similar to those observed at the initial survey, they were generally lower, indicating further reduction in contamination over time [7]. The geoelectric images now exhibited a shift from green to blue and dark blue, which signifies a continued decrease in resistivity and greater hydrocarbon breakdown [54].

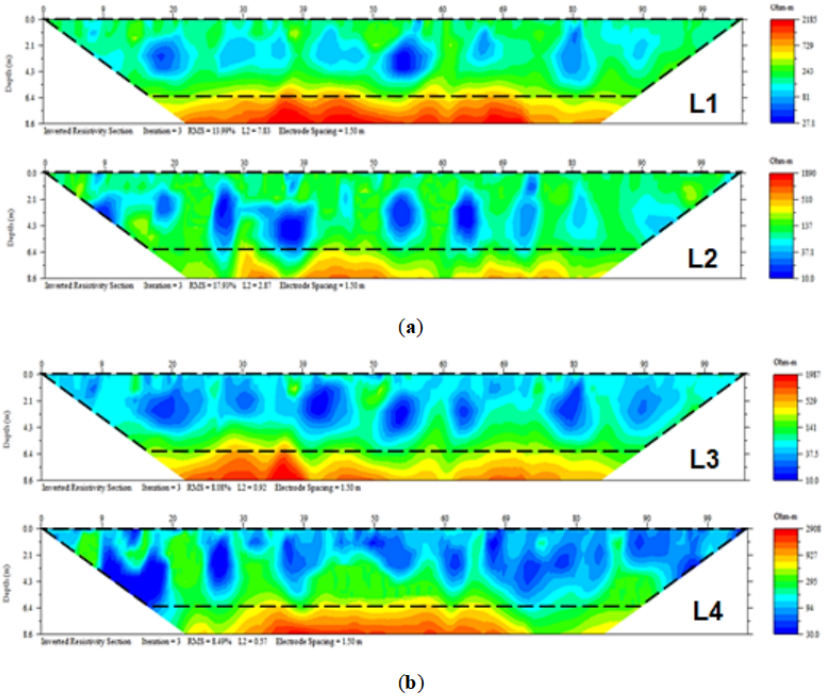


**Figure 4.** (**a**) First phase survey geoelectric image for L1 and L2; (**b**) Second phase survey geoelectric image for L3 and L4.

This trend suggests that biodegradation and natural attenuation processes continued to act effectively over the six months, with an observed relative decrease in resistivity values through both survey phases, indicating that the degradation process has considerably reduced hydrocarbon contamination [7]. Line 4, which had the most significant resistivity reduction, demonstrated the most considerable improvement, followed by Line 3. This implies that Line 4 experienced the most effective attenuation and continued biodegradation, particularly in the near subsurface regions above 3 m. These areas exhibited the highest atmospheric interaction, facilitating aerobic activities and enhancing microbial organic digestion and hydrocarbon degradation [14]. It is also evident that biodegradation occurs more significantly in the subsurface areas closer to the ground within the zone of active biodegradation and contaminant mass reduction,

compared to deeper depths [7]. This is represented by the shift from green to blue and dark blue in the second phase survey images, covering previously predominantly green areas in the first phase images. Line 4, showing the biggest improvement, might have benefited from more effective treatment conditions or more favourable natural attenuation mechanisms [6], while Line 3 displayed moderate improvement, indicating ongoing effective but not optimal attenuation. This shift aligns with the characteristic of hydrocarbon-contaminated soils, where older contaminants exhibit low resistivity values due to their degradation and breakdown [60]. The variability in resistivity changes among the different lines highlights spatial differences in the biodegradation dynamics.

## 4.2. Temporal Biodegradation Assessment of Soil TPH

Over six months spanning the first and second phases of sampling, degradation has notably reduced TPH contents in soils. The values of TPH during the first phase sampling were between 26.74 mg/kg for SC-6 of BH2 at 5.0 m and 182.17 mg/kg for SC-3 of BH1 at 5.0 m. At the same time, the values of TPH for the second sampling phase range between 15.17 mg/kg for SC-10 of BH4 at 0.5 m and 98.66 mg/kg for SC-9 of BH3 at 5.0 m (**Table 5**). The assessment encompasses the TPH concentrations for hydrocarbon categories C6–C10 and C10–C40 across boreholes BH1, BH2, BH3, and BH4 and depths of 0.5 m, 3.0 m, and 5.0 m. The first phase sampling showed noticeable TPH concentrations in at least one depth across both boreholes (**Figure 5a**), while the second phase sampling exhibited lower TPH levels in almost all of the samples (**Figure 5b**).

The spatiotemporal attenuation assessment for BH1 and BH3 showed drops in TPH levels from 103.00 mg/kg to 42.57 mg/kg at 0.5 m depth, implying a > 58% decrease in the contamination level. At the 3.0 m depth, there was also a decrease from 36.83 mg/kg to 29.64 mg/kg, indicating a > 19% decline in the TPH concentration. The 5.0 m depth also decreased from 182.17 mg/kg to 98.66 mg/kg, which makes up for a > 45% decline in the TPH levels. For the BH2 and BH4, there was a drop in TPH levels from 42.57 mg/kg to 15.17 mg/kg at 0.5 m, which is > 64% decrease in the TPH concentrations, mirroring similar huge drops in contaminants mass of SC-1 at 0.5 m; this implies active biodegradation at shallow subsurface areas closest to the ground due to suitable conditions favouring aerobic hydrocarbon breakdown [17]. For SC-5 at 3.0 m depth, there was also a decrease in contamination levels from 111.27 mg/kg to 84.39 mg/kg, representing a decrease in TPH concentrations by > 24%. In contrast with these other findings, results obtained from BH4 at 5.0 m depths showed a trend difference, which indicated a reverse in contamination levels, recording a 16% increase in TPH concentrations from 26.74 mg/kg at BH2 to 31.94 mg/kg at BH4. The TPH trend of BH4 at 5.0 m indicates potential recontamination from the spill source due to subsurface contaminant migration along a possible subsoil water flow pathway [34]. Generally, there were exclusively TPH contaminations from the C10–C40 fractions across the samples, with the C6–C10 degraded and remaining consistently < 0.1 mg/kg in all the second phase samples; this implies a significant reduction in the heavier hydrocarbons, with the light hydrocarbons all below negligible limits [3].

**Table 5.** Geochemical analysis for the soils.

| Sample I.D. | Reference | Depth (m) | Sampling | C10–C40 (mg/kg) | C6–C10 (mg/kg) | TPH (mg/kg) |
|---|---|---|---|---|---|---|
| SC-1 | | 0.5 | | 103.00 | < 0.1 | 103.00 |
| SC-2 | BH 1 | 3.0 | | 36.83 | < 0.1 | 36.83 |
| SC-3 | | 5.0 | First Phase | 182.05 | 0.19 | 182.17 |
| SC-4 | | 0.5 | | 40.93 | 1.64 | 42.57 |
| SC-5 | BH 2 | 3.0 | | 111.27 | < 0.1 | 111.27 |
| SC-6 | | 5.0 | | 26.74 | < 0.1 | 26.74 |
| SC-7 | | 0.5 | | 43.75 | < 0.1 | 43.75 |
| SC-8 | BH 3 | 3.0 | | 29.64 | < 0.1 | 29.64 |
| SC-9 | | 5.0 | Second Phase | 98.66 | < 0.1 | 98.66 |
| SC-10 | | 0.5 | | 15.17 | < 0.1 | 15.17 |
| SC-11 | BH 4 | 3.0 | | 84.39 | < 0.1 | 84.39 |
| SC-12 | | 5.0 | | 31.94 | < 0.1 | 31.94 |
| DPR (EGASPIN, 2018) | | | Permissible Level / Target Limit | | | 50.00 |

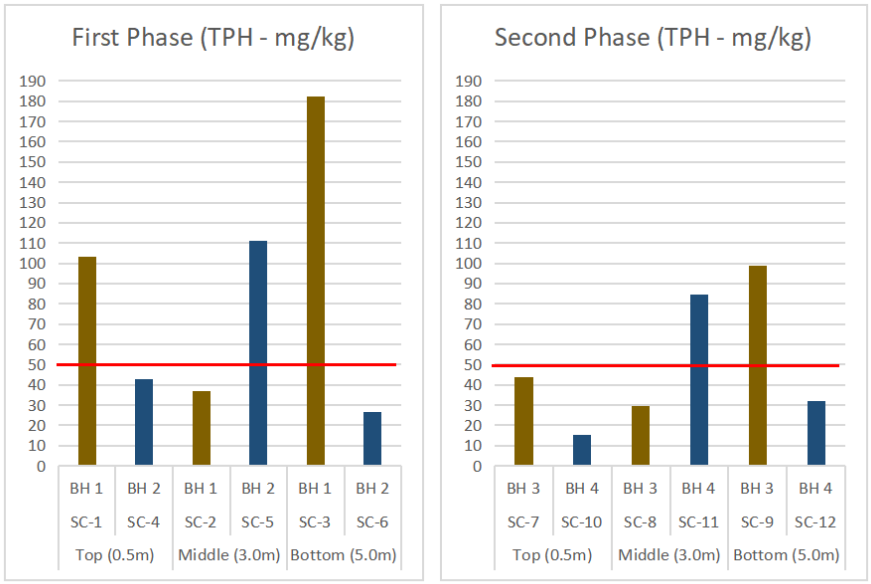


**(a)** **(b)**

**Figure 5.** (**a**) First phase sampling for BH 1 and BH 2; (**b**) Second phase sampling for BH 3 and BH 4.

Degradation occurs more significantly in the shallowest subsurface areas closer to the ground, corresponding with the zone of active biodegradation and contaminant mass reduction than in deeper depths[4]. The decrease in TPH levels reflects progress in attenuation, leading to improved soil quality[36], particularly in regions exhibiting the highest atmospheric interaction, facilitating aerobic activities and enhancing microbial organic digestion and hydrocarbon degradation[61]. However, C10–C40 levels at 5.0 m for BH3 and 3.0 m for BH4 still exceed regulatory limits of 50 mg/kg for hydrocarbon concentration in soils according to the Department of Petroleum Resources (DPR)–Environmental Guidelines and Standards for the Petroleum Industry in Nigeria[49]. The degradation monitoring revealed a 19% to 64% reduction in average TPH concentrations from the first to the second phases of sampling. However, despite these improvements, the remaining TPH concentrations for C10–C40 still exceed the DPR limits in some areas, especially closer to the pipeline and further away below 3.0 m, indicating that while significant progress has been made, complete attenuation has not yet been achieved[62]. This suggests ongoing risks to human health, including potential long-term exposure to harmful hydrocarbons, particularly through groundwater contamination, since most residual impacts are attributed to more profound subsurface occurrences[3]. Although the partial reduction in contamination benefits and supports better soil and environmental quality by improving soil health and reducing the risk of further ecological damage, residual contamination can still impact plant growth and disrupt local ecosystems[9]. Lower contamination levels are favourable for restoring plant growth, environmental balance, and engineering competence[51].

## 4.3. Evaluation of Soil Mechanical Properties

### 4.3.1. Specific Gravity Test

The laboratory analysis results for specific gravity offer valuable insights into the density characteristics of the soil samples. The specific gravity (Gs) values for some minerals include Calcite (2.72), Feldspar (2.55 to 2.76), Kaolinite (2.61), Quartz (2.65), Montmorillonite (2.74), Muscovite (2.7 to 3.1), and Xylotile (2.4 to 2.55)[35,63]. The distribution of specific gravity among the samples (**Figure 6**) illustrates trends in Gs values, resulting from similarities in soil types despite variations in composition, with each sample assigned an average specific gravity value, with notable distinctions observed among the various samples. Gs values for the samples range from 2.47 to 2.60, averaging at approximately 2.49, suggesting that the soils belong to the feldspar mineral range and are classified as moderate to light soils[64].

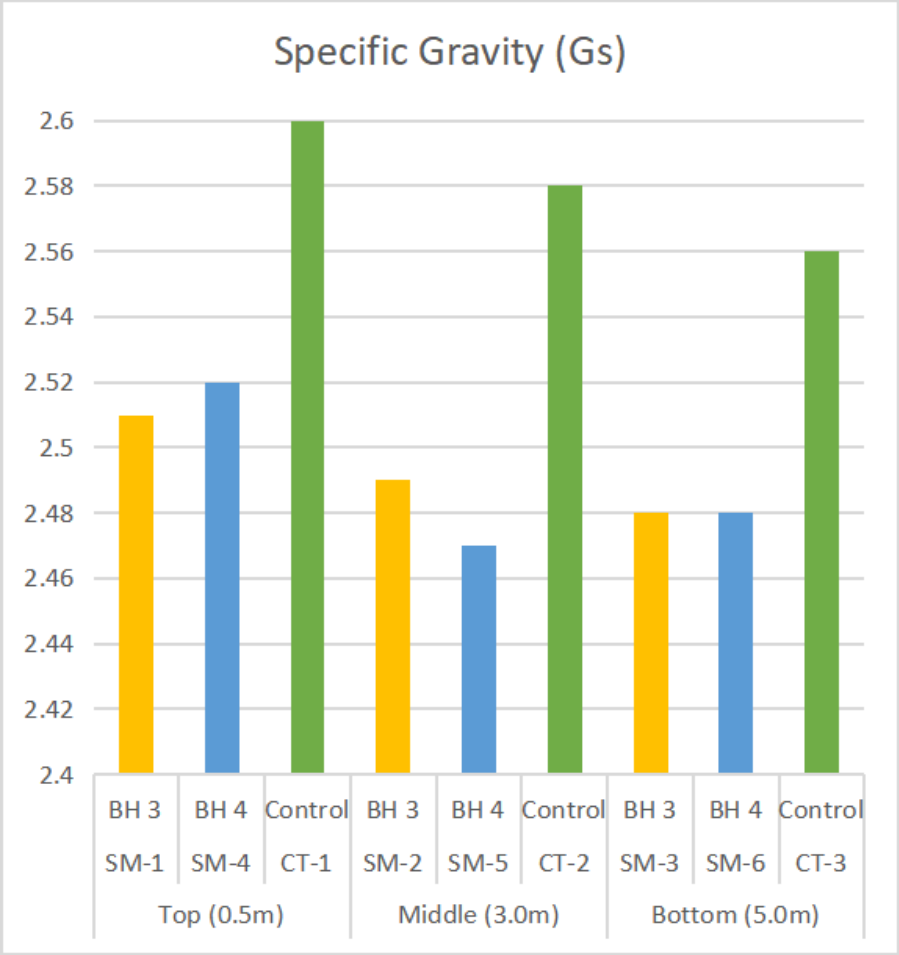


**Figure 6.** Specific gravity for BH 3, BH 4, and control (BH 5).

SM-1 and SM-4 stand out amongst other samples with specific gravity values of 2.51 and 2.52, respectively. This disparity is attributed to their composition, characterized by higher sand and gravel proportions [65] than samples SM-2, SM-3, SM-5, and SM-6. The elevated coarse particles in SM-1 and SM-4 contribute to their relatively lower specific gravity values than the other samples. **Table 6** summarizes the specific gravity of both the control and second-phase sampled soils. The control samples exhibit higher specific gravity values, with CT-1, CT-2, and CT-3 recording values of 2.6, 2.58, and 2.56, respectively. This difference suggests variations in composition between the control and impacted samples, with the control samples potentially containing denser materials or a different distribution of particle sizes [64]. Overall, the specific gravity analysis underscores the importance of considering soil samples' composition and density characteristics in understanding their properties and behaviour [66]. The distinct values observed among the samples highlight the variability inherent in soil composition and its implications for engineering and environmental applications [67]. The specific gravity test is a fundamental soil test used to determine the density of soil particles, which is crucial for understanding soil properties such as compaction, porosity, and stability [51]. The results provide insights into soil composition and can be used to infer the potential impacts of hydrocarbon contamination on soil behaviour and degradation efforts [67].

For BH3, SM-1 at 0.5 m, the TPH value is 43.75 mg/kg, with a specific gravity of 2.51, indicating dense soil with significant mineral content [64]. The soil composition is influenced by the presence of hydrocarbons but maintains stability. SM-2 at 3.0 m had a TPH value decrease to 29.64 mg/kg, with the specific gravity slightly reduced to 2.49, suggesting minor alterations in soil density due to degradation or hydrocarbon impact [66]. SM-3 at 5.0 m, although with a relatively higher TPH value of 98.66 mg/kg, had its specific

gravity drop to 2.48, indicating the potential effects of higher hydrocarbon concentration on soil compaction and mineral density[65]. For BH4, SM-4 at 0.5 m depth had a TPH value of 15.17 mg/kg and a specific gravity of 2.52, showing a dense soil composition with a slight TPH influence[66]. SM-5 at 3.0 m had a TPH spike of 84.39 mg/kg, with a specific gravity of 2.47, indicating minor effects on soil density from hydrocarbon presence[63]. SM-6 at 5.0 m with a TPH value of 31.94 mg/kg retained a consistent specific gravity of 2.48 with SM-3 at 5.0 m depth, suggesting stable soil density despite changes in hydrocarbon concentrations[67]. For the control samples (BH5), CT-1 at 0.5 m had a specific gravity of 2.60, suggesting higher mineral content or compaction[51]. CT-2 and CT-3 at 3.0 m and 5.0 m, with a specific gravity of 2.58 and 2.56, respectively; these closely related Gs values for the control samples indicate a stable reference for soil density averaging at 2.58 and provide baseline conditions for comparison and evaluation.

**Table 6.** Specific gravity of the soils.

| Sample I.D. | Profile | | Specific Gravity (Gs) |
|---|---|---|---|
| | Reference | Depth (m) | |
| SM-1 | BH 3 | 0.5 | 2.51 |
| SM-2 | | 3.0 | 2.49 |
| SM-3 | | 5.0 | 2.48 |
| SM-4 | BH 4 | 0.5 | 2.52 |
| SM-5 | | 3.0 | 2.47 |
| SM-6 | | 5.0 | 2.48 |
| CT-1 | Control BH 5 | 0.5 | 2.60 |
| CT-2 | | 3.0 | 2.58 |
| CT-3 | | 5.0 | 2.56 |

The analysis of specific gravity values in degradation or attenuation soils indicates a slight decrease in soil density with increased TPH concentrations[63]. The consistency of specific gravity in BH3 and BH4 across the 5.0 m depths suggests minimal impact from hydrocarbon presence. Control samples demonstrate a higher specific gravity range, reflecting natural soil mineral content and compaction variability[65]. The Gs for the second phase sampling averages at approximately 2.49, corresponding with the Xylotile mineral associated with organic matter, fibrous, lightweight structure, and water-absorption properties[66]. This contrasts with the control sample average at 2.58, falling within the feldspar minerals, typically associated with most sandy, silty, or clayey soils, contributing to moderate to high soil strength and stability. This implies that the soils now wholly fall into the classification of light to very light soils[67], suggesting that hydrocarbon contaminations and degradation efforts have considerably altered the soil density, indicating relative instability due to ongoing degradation and corresponding organic alterations in soil conditions[51].

### 4.3.2. Particle Size Distribution Analysis

The particle size distribution and soil description, summarised in **Table 7**, were assessed using the Unified Soil Classification System[35] and the American Association of State Highway and Transportation Officials[53]. The USCS utilizes symbols to represent different soil types, including Gravel (G), Sand (S), Silt or Silty (M), Clay or Clayey (C), Organic (O), Peat (Pt), Well graded (W), and Poorly graded (P). Fifty percent or more of the coarse fraction passing through the 4.75 mm sieve is termed Sand[35]. Coarse-grained soils are classified into GW (Well-graded Gravel), GP (Poorly graded Gravel), SW (Well-graded Sand), SP (Poorly graded Sand), SM (Silty Sand), GM (Silty Gravel), SC (Clayey Sand), and GC (Clayey Gravel). Fine-grained soil is characterized by 50% or more passing through a 0.075 mm sieve[35]. **Figure 7** provides the distribution chart regarding the particle sizes of soil samples taken from the study site at BH3 and BH4 and the control site at BH5. This analysis aids in understanding the physical characteristics of the soil and its implications for water retention and flow dynamics[13]. Samples SM-3, SM-6, SM-5, and SM-2 exhibit similar proportions of gravel, sand, and silt/clay, with a notable predominance of silt/clay over sand. This composition suggests a tendency towards water retention, slowing down water flow within these samples[52]. However, SM-1 displays different characteristics, with higher levels of gravel and sand than the other samples. This composition facili-

tates better water flow and lower water retention capacities than the samples[68].

**Table 7.** Summary of the particle size distribution of the soils.

| Sample I.D. | Reference | $D_{10}$ (mm) | $D_{30}$ (mm) | $D_{60}$ (mm) | Cu (mm) | Cc (mm) | Grain Size Analysis (%) | | |
|---|---|---|---|---|---|---|---|---|---|
| | | | | | | | Gravel | Sand | Clay |
| SM-1 | BH 3 | 0.0045 | 0.017 | 0.32 | 71.1 | 0.20 | 1.62 | 47.85 | 50.53 |
| SM-2 | | 0.004 | 0.014 | 0.19 | 47.5 | 0.0026 | 0.66 | 42.03 | 57.31 |
| SM-3 | | 0.0035 | 0.0095 | 0.07 | 20 | 0.37 | 0.53 | 33.57 | 65.89 |
| SM-4 | BH 4 | 0.0039 | 0.018 | 0.32 | 82.05 | 0.026 | 1.59 | 49.57 | 48.83 |
| SM-5 | | 0.0031 | 0.0085 | 0.069 | 22.2 | 0.34 | 0.61 | 37.06 | 62.33 |
| SM-6 | | 0.0030 | 0.011 | 0.65 | 20.97 | 0.6 | 0.67 | 34.09 | 65.23 |
| CT-5 | Control BH 5 | 0.17 | 0.33 | 0.46 | 2.71 | 1.39 | 8.97 | 85.29 | 5.74 |
| CT-6 | | 0.07 | 0.31 | 0.45 | 6.4 | 3.05 | 6.89 | 81.50 | 11.61 |
| CT-7 | | 0.12 | 0.030 | 0.40 | 3.33 | 1.875 | 2.21 | 92.65 | 5.14 |

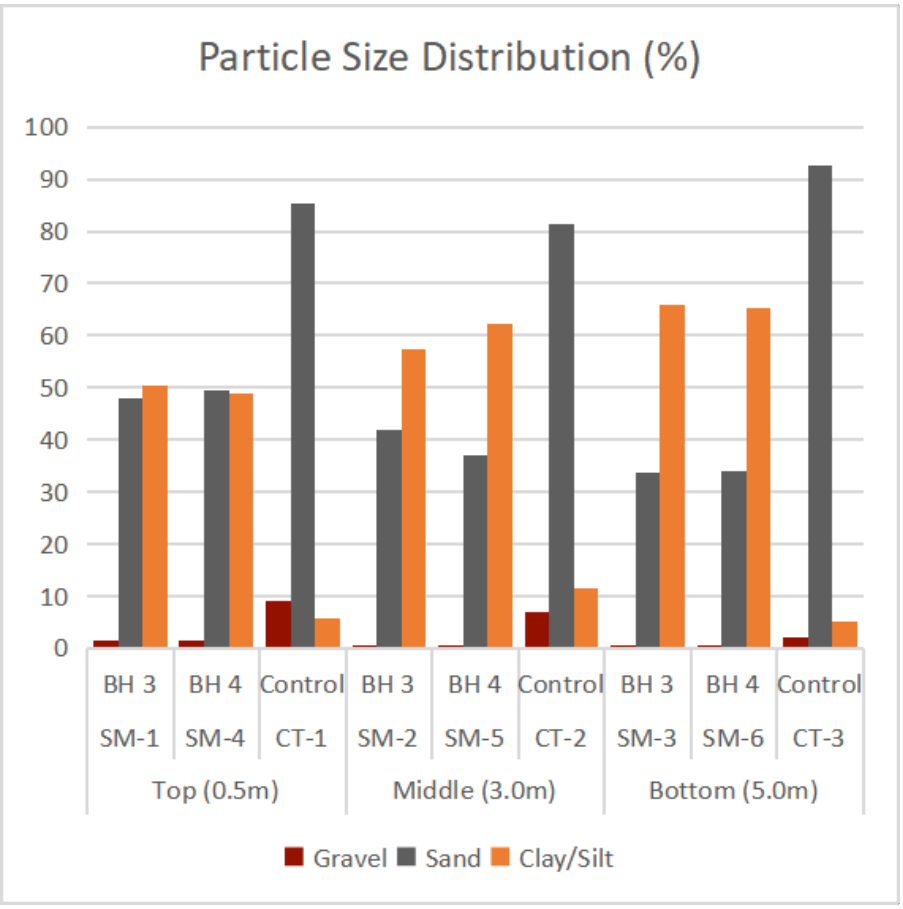


**Figure 7.** Particle size distribution for BH 3, BH 4, and control (BH 5).

Notably, SM-4 stands out as it falls under the classification of clayey sand according to the Unified Soil Classification System[35]. It exhibits a higher ratio of sand and gravel (49.57% sand, 1.59% gravel) with 48.83% silt/clay. The result of the hydrometer test indicates a silt and clay proportion of 4%. This composition suggests lower water retention capabilities and higher water flow rates, thereby affecting the distribution and retention of chemicals within the soil[11]. **Figures 8** and **9** illustrate the particle size distribution curves, which combine sieve analysis and hydrometer test data for both the second phase and control samples, presenting a graphical representation of the analysis trend.

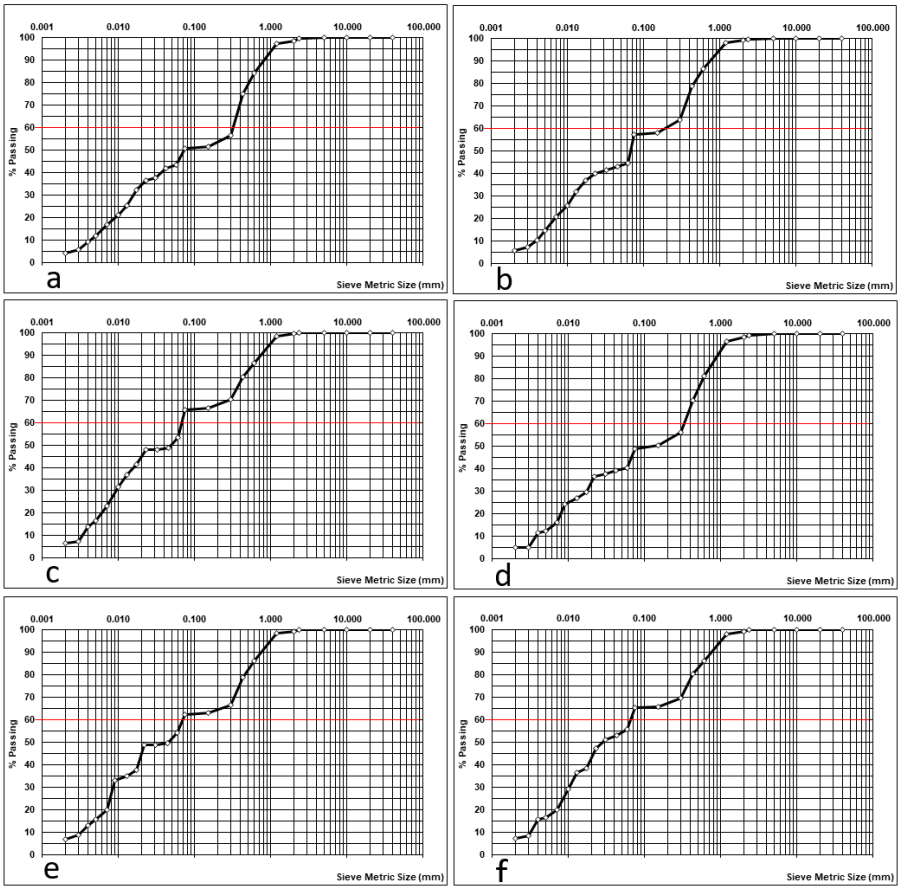


**Figure 8.** Particle size distribution curve for BH 3 and BH 4.

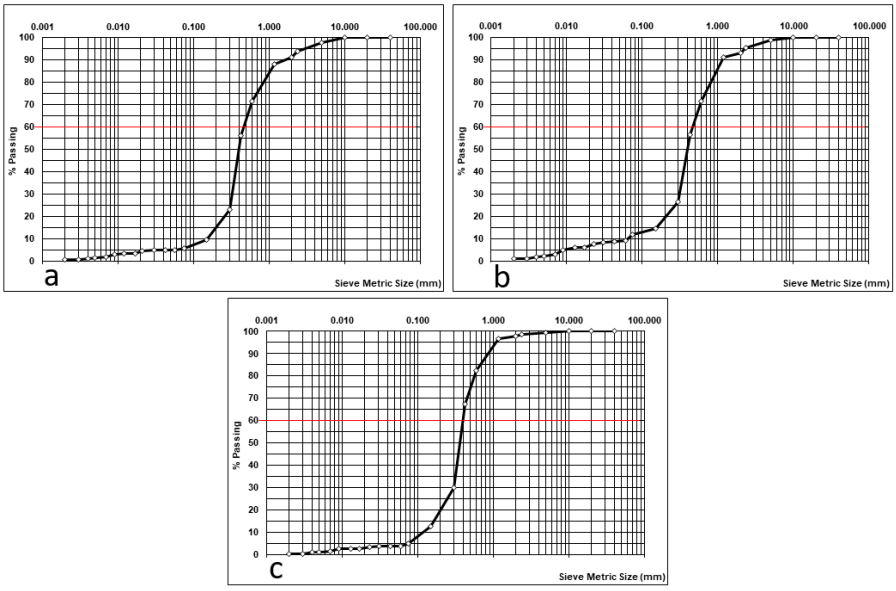


**Figure 9.** Particle size distribution curve for control (BH 5).

Contrary to the study site, the control demonstrates varying particle sizes, with higher proportions of sand and gravel than clay. This composition promotes fluid movement through the soil medium, facilitating better drainage and lower water retention capacities [67] than the second phase samples. The differences observed in particle size distribu-

tion between the attenuation site and control samples have significant implications for water retention, flow dynamics, and chemical distribution within the soil[65]. While the study site exhibits higher silt/clay content, leading to more excellent water retention and slower flow rates, the control samples demonstrate improved drainage capabilities due to higher sand and gravel content[35]. For BH3, sample SM-1 at 0.5 m depth indicates a predominance of silt and clay (50.53%), classifying it as Sandy Lean Clay[35] and A-4 (2)[53]. Fine-textured soil shows high plasticity, affecting drainage and compaction, with low permeability and challenges from shrink-swell behaviour[57]. Sample SM-2, at a depth of 3.0 meters, displays similarity to SM-1, with 57.31% silt and clay. Its classification as Sandy Lean Clay[35] and A-4 (2)[53] suggests low permeability and potential shrink-swell behaviour, necessitating careful remediation to manage contaminant transport and water retention[11]. Sample SM-3 at 5.0 m depth has 65.89% fines, also falling into the Sandy Lean Clay[35], with A-4 (4)[53] category. The high fines content indicates low permeability, which impacts drainage and compaction and requires remediation strategies to ensure soil stability[11].

For BH4, the sample SM-4 at 0.5 m depth is classified as Clayey Sand[35] and A-4 (1)[53], with 48.83% fines with enhanced permeability due to its higher sand content[51]. This aids drainage but requires attention to stability and erosion in remediation plans[65]. Sample SM-5 at 3.0 m depth indicates Sandy Lean Clay[35] and A-4 (4)[53], characterized by a high percentage of fines, low permeability, and potential water retention impacting drainage and stability, necessitating effective soil management strategies[67]. Sample SM-6 at a depth of 5.0 meters is also similar to SM-5. It is classified as Sandy Lean Clay[35] and A-4 (5)[53] with high fines content, requiring tailored remediation to manage permeability and stability[11]. For BH5, at the control site, sample CT-1 at 0.5 m depth is classified as Poorly-graded Sand with Silt[35] and A-3 (0)[53]; it shows high permeability and low water retention, necessitating erosion and drainage[14]. Sample CT-2 at 3.0 m depth has a sandy texture and moderate fines, classified as Poorly-graded Sand with Silt[35] and A-2-4 (0)[53]. Sample CT-3 at 5.0 m depth falls under the USCS[35] classification as Poorly-graded Sand with Silt and A-3 (0)[53]. The analysis of the control site presents the original soil properties, and its textural composition and distributions align with previous findings by Amadi[58], Ovuru and Udom[55], and Nwankwoala & Mzaga[11]. The results reflect the significant effects of TPH contamination and alterations in attenuation site soils compared to the control site, with BH3 showing the highest TPH concentration at 5.0 m (98.66 mg/kg), indicating significant hydrocarbon presence and lower values at 0.5 m (43.75 mg/kg) and 3.0 m (29.64 mg/kg), respectively corresponding to the different high plasticity dynamics[67], potentially affecting drainage and compaction, with low permeability and shrink-swell behaviour challenge[4]. Also, BH4 exhibits similar properties corresponding to the varied TPH levels, implying that TPH concentrations contributed to increased soil plasticity and reduced permeability, altering compaction characteristics, water retention, and permeability[67], with higher TPH concentrations directly correlating to higher soil plasticity[63].

### 4.3.3. Consolidation Tests

Consolidation occurs when water is expelled from these voids, compressing the soil mass[51]. Consolidation accounts for the entire settlement process in saturated soils, as there is no additional compaction due to the absence of air-filled voids[67]. **Table 8** summarizes the pre-consolidation stress of the test results for all samples. **Figures 10** and **11** display the chart depicting the comparison of the average settlement and coefficient of consolidation versus the applied stresses for all the samples, presenting the generalized visual representation of the analysis trends for BH3, BH4, and control (BH5), offering critical insights into their characteristics. These values reflect the soil's ability to retain water and its flow properties following the load application[51]. **Figures 12** and **13** illustrate the consolidation curves for the second phase and control sampling, respectively.

Among the BH3 and BH4 second-phase samples, SM-3, SM-5, and SM-6 exhibit high levels of saturation, indicative of their clay content's capacity to retain water, coupled with sand and gravel's relatively lower water retention[51]. BH5 control samples CT-1, CT-2, and CT-3 demonstrate lower saturation levels, reflecting their composition dominated by sand and gravel, facilitating efficient drainage and lower water retention[24]. Understanding soil samples' consolidation behaviour and saturation characteristics is essential for assessing their stability and deformation under load[4]. The observed differences between the second phase and control samples provide valuable insights into the effects of hydrocar-

bon contamination, the effectiveness of attenuation efforts, and the soil's response to applied loads[67]. Further analysis and interpretation of these results can inform engineering decisions and design considerations for various soil-related projects[51]. The consolidation test evaluates the soil's ability to change volume under applied loads, providing insights into the compressibility and settlement characteristics[60]. The results from samples SM-1 to SM-6 and control samples CT-1 to CT-3 offer an understanding of their consolidation behaviour, which is critical for predicting the long-term settlement of structures built on these soils[24]. Evaluation and correlation of the samples show that for BH3, sample SM-1 at 0.5 meters depth, the overall settlement was 2.112 mm, with a final void ratio of 0.453, indicating moderate compressibility[67]. The initial saturation was high at 108.77%, decreasing to 82.56% after the test. The pre-consolidation stress was measured at 143 kN/m², suggesting the soil had undergone previous loading[31].

**Table 8.** Summary of consolidation tests of the soils.

| Sample I.D. | Profile | | Pre-Consolidation Stress (kN/m²) |
|---|---|---|---|
| | Reference | Depth (m) | |
| SM-1 | BH 3 | 0.5 | 143 |
| SM-2 | | 3.0 | 134 |
| SM-3 | | 5.0 | 128 |
| SM-4 | BH 4 | 0.5 | 148 |
| SM-5 | | 3.0 | 140 |
| SM-6 | | 5.0 | 161 |
| CT-1 | Control BH 5 | 0.5 | 115 |
| CT-2 | | 3.0 | 140 |
| CT-3 | | 5.0 | 129 |

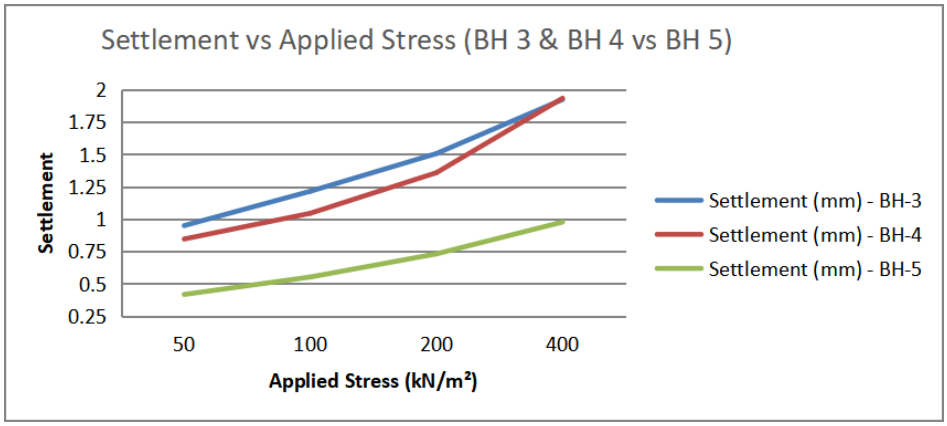


**Figure 10.** Settlement comparison with applied stress.

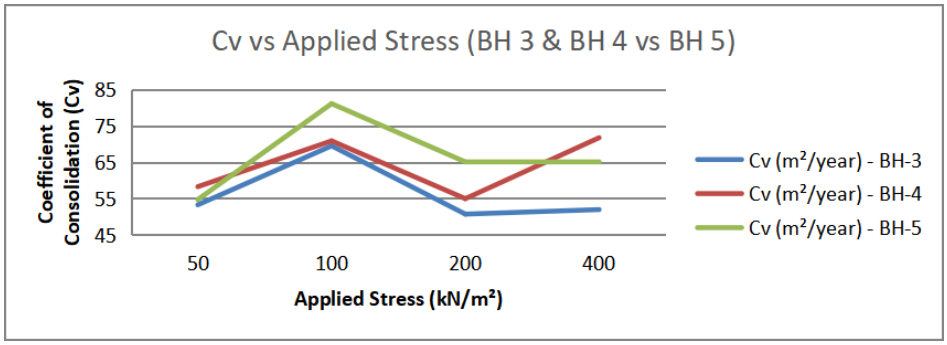


**Figure 11.** Coefficient of consolidation comparison with applied stress.

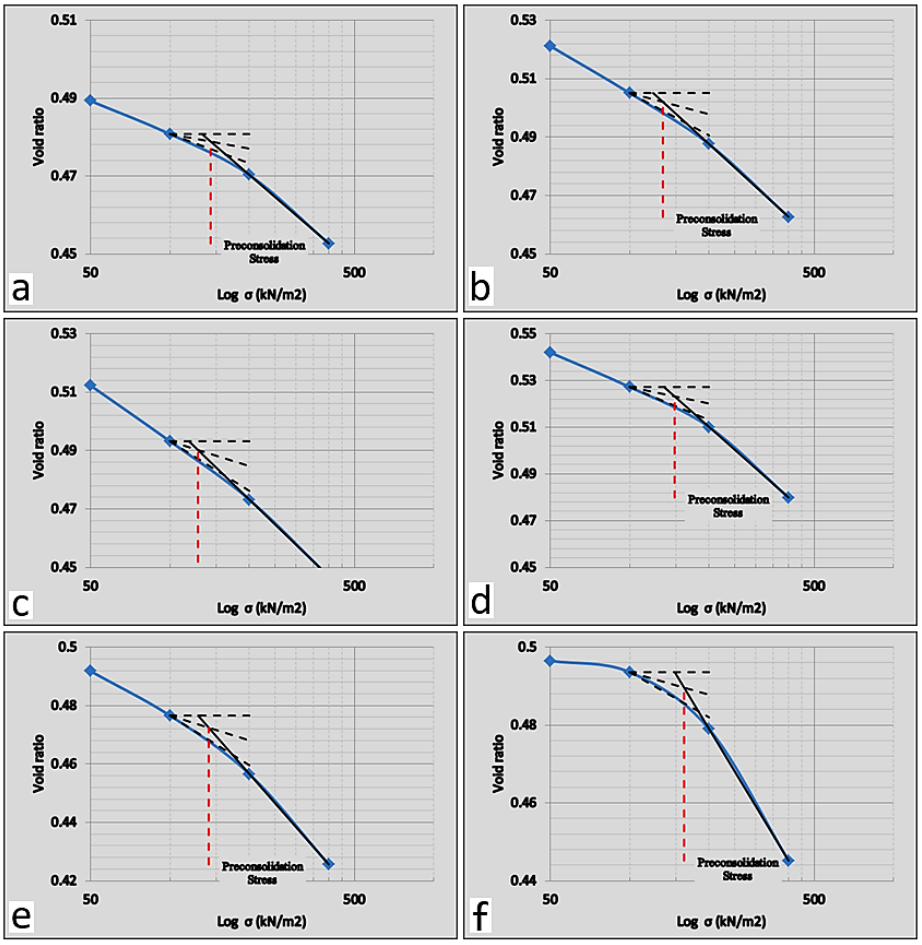


**Figure 12.** Consolidation curve for BH 3 and BH 4.

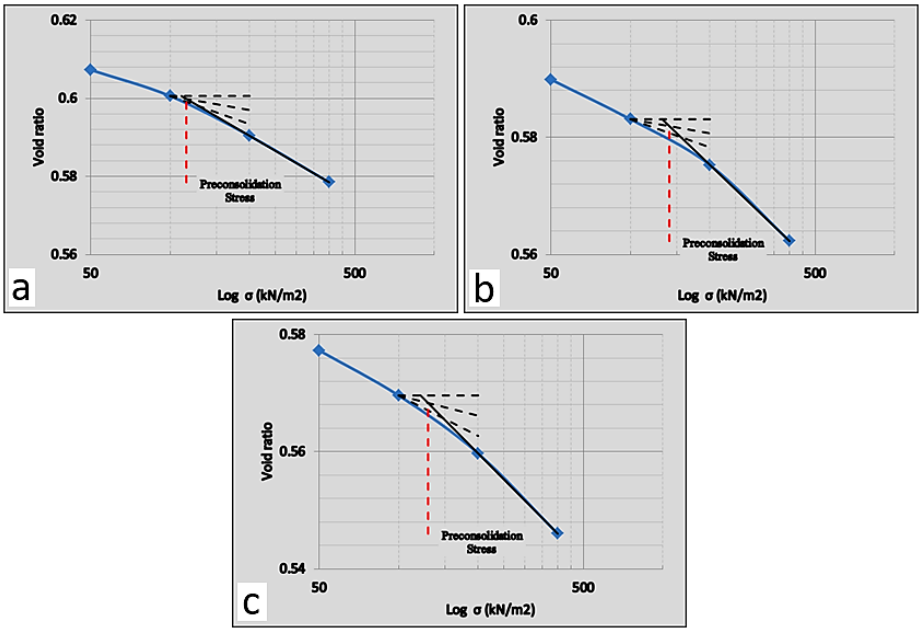


**Figure 13.** Consolidation curve for control (BH 5).

For SM-2 at a depth of 3.0 meters, the sample showed an overall settlement of 1.78 mm and a final void ratio of 0.463. Initial saturation was 109.83%, decreasing to 80.13% post-test. With a consolidation stress of 134 kN/m$^2$, this sample exhibited slightly less compressibility than SM-1, indicating effective degradation impacts on soil structure [24]. For sample SM-3 at 5.0 meters depth, the overall settlement was 1.876 mm, with a final void ratio of 0.447. The initial saturation of 111.37% decreased to 82.67% post-test. The pre-consolidation stress was 128 kN/m$^2$, suggesting moderate compressibility [67]. For BH4, sample SM-4 at 0.5 meters depth, the overall settlement was 1.831 mm, with a final void ratio of 0.48. Initial saturation was 107.32%, dropping to 78.23% post-test. The pre-consolidation stress was 148 kN/m$^2$, indicating moderate compressibility and effective degradation impacts [4]. SM-5 at a depth of 3.0 meters, this sample had an overall settlement of 2.059 mm and a final void ratio of 0.426. The initial saturation was 112.98%, with a final saturation of 86.39%. The pre-consolidation stress was 140 kN/m$^2$, reflecting a higher compressibility than other depths [51]. SM-6 at 5.0 meters depth, the overall settlement was 1.907 mm, with a final void ratio of 0.445. The initial saturation was 111.37%, decreasing to 83.04% post-test. The pre-consolidation stress was 161 kN/m$^2$, indicating a well-compacted structure with moderate compressibility [13].

Concerning BH5 at the control site, sample CT-1 at 0.5 m depth, the overall settlement was 0.984 mm, with a final void ratio of 0.579. Initial saturation was 101.94%, decreasing to 66.91%. The pre-consolidation stress was 115 kN/m$^2$, showing low compressibility [51]. CT-2 at 3.0 m depth, the overall settlement was 0.915 mm, with a final void ratio of 0.562. Initial saturation was 104.47%, reducing to 68.4%. The pre-consolidation stress was 140 kN/m$^2$, reflecting low compressibility and high resistance to settlement [24]. Sample CT-3 at 5.0 m depth, the overall settlement was 1.031 mm, with a final void ratio of 0.546. Initial saturation was 105.39%, reducing to 69.86%. The pre-consolidation stress was 129 kN/m$^2$, indicating low compressibility [51]. The results show that TPH contamination affects the consolidation characteristics of soil by altering its structure and compressibility [13]. Samples from BH3 showed increased settlement with depth, corresponding to higher TPH concentrations, particularly in SM-1 and SM-3, indicating that contamination has contributed to higher compressibility [67]. In BH4, samples exhibited varied settlement values, with SM-5 showing the highest settlement, suggesting that remediation efforts must focus on managing compressibility to enhance soil stability [64].

The comparative analysis of the consolidation test results reveals a clear distinction between hydrocarbon-contaminated and uncontaminated soils. Both BH3 and BH4 (contaminated) exhibit higher settlement than BH5 (control), indicating a loss of soil strength and increased compressibility due to contamination [10]. Notably, BH3 experiences slightly more significant settlement than BH4, suggesting that the contamination effects are more pronounced at BH3. The coefficient of consolidation (Cv) trends further supports this observation [29]. BH3 and BH4 both show lower Cv values than BH5, indicating slower consolidation rates due to reduced permeability in contaminated soils [51]. This slower consolidation is attributed to the hydrocarbon-induced alteration of soil structure, which affects drainage and settlement behavior [13]. Among the contaminated boreholes, BH4 exhibits a slightly higher Cv than BH3, suggesting that the degree of contamination at BH4 may be less severe than at BH3 [69]. The findings confirm that hydrocarbon contamination significantly alters soil consolidation properties, leading to increased settlement and reduced consolidation rates [63]. These changes highlight the potential geotechnical challenges associated with contaminated sites, particularly in foundation stability and long-term soil performance [11].

## 4.4. Geochemical and Geotechnical Correlation

The correlation analysis between Total Petroleum Hydrocarbon (TPH) content and geotechnical properties (specific gravity, consolidation parameters, and particle size distribution) for BH3 (**Figure 14**) and BH4 (**Figure 15**) at different depths (Top, Mid, Base). The analysis and visualization were done using Python-based scientific visualization libraries, incorporating Matplotlib, SciPy, and Seaborn [10]. The analysis reveals distinct interactions between contamination levels and soil behaviour [13], with both boreholes exhibiting changes in compressibility, consolidation behaviour, and particle size characteristics due to hydrocarbon contamination.

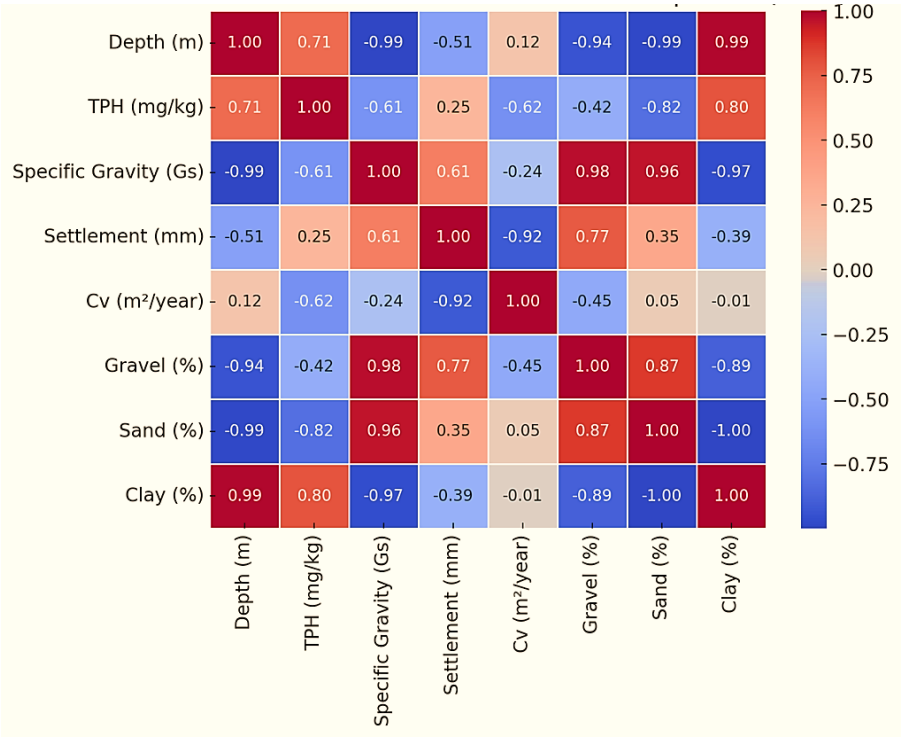


**Figure 14.** Correlation analysis of geochemical against geotechnical properties for second phase (BH 3).

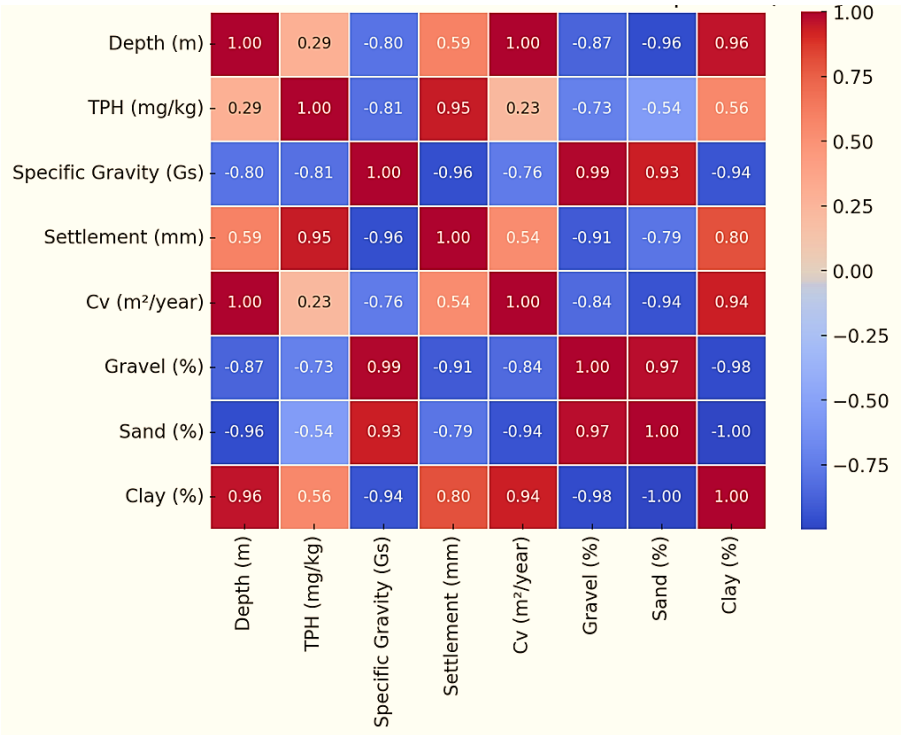


**Figure 15.** Correlation analysis of geochemical against geotechnical properties for second phase (BH 4).

In BH3, a weak positive correlation (0.25) between TPH and settlement suggests that higher TPH concentrations slightly increase soil compressibility, potentially weakening the soil structure[70]. Conversely, the coefficient of consolidation (Cv) has a moderate negative correlation (−0.62) with TPH, indicating that soils with higher TPH levels consolidate

more slowly[51]. This reduction in consolidation rate may be due to hydrocarbons altering permeability and drainage, leading to prolonged settlement periods[4]. In contrast, BH4 exhibits a much stronger positive correlation (0.95) between TPH and settlement, indicating that higher TPH levels significantly increase soil compressibility[50]. Unlike BH3, the effect of TPH on Cv in BH4 is minimal (0.23), suggesting that hydrocarbon contamination does not significantly alter the rate at which the soil consolidates[66].

Specific gravity is negatively correlated with TPH in both boreholes, although the effect is more pronounced in BH4 (−0.81) than in BH3 (−0.61). This trend suggests that higher contamination levels tend to lower the soil density[33], likely due to hydrocarbons replacing water in the soil pores[67]. The impact of TPH on particle size distribution also varies between the boreholes. In BH3, there is a strong positive correlation (0.79) with clay content and a strong negative correlation (−0.82) with sand content, indicating that higher contamination levels are associated with finer soil particles[65]. A similar but slightly weaker trend is observed in BH4, where TPH has a moderate positive correlation (0.56) with clay and a mild negative correlation (−0.54) with sand[12].

Additionally, gravel content shows a moderate to strong negative correlation with TPH in both BH3 (−0.42) and BH4 (−0.72), reinforcing the trend that contaminated soils tend to have fewer coarse particles and a more significant proportion of fines[70]. The hydrocarbon contamination altered the geotechnical properties of the soils in both boreholes, but with varying degrees of impact. BH3 shows slower consolidation and moderate changes in settlement, while BH4 exhibits a much more substantial increase in settlement but retains its consolidation rate. In both cases, contaminants preferentially interact with finer soil particles, reducing specific gravity and altering the soil's physical and mechanical behaviour[51]. These findings have significant implications for foundation stability, soil remediation strategies, and long-term geotechnical performance in hydrocarbon-contaminated sites.

## 4.5. Geoenvironmental and Geoengineering Profiling

The geoenvironmental and geoengineering profiling conducted in this study provides critical insights into the interplay between Total Petroleum Hydrocarbon (TPH) contamination and soil geotechnical properties, as well as the effects of contaminants attenuation. **Table 9** provides a summary of the geoenvironmental and geoengineering profiling of the study site. Specific gravity analysis revealed that attenuation soils exhibited values ranging from 2.47 to 2.52, while control samples recorded higher values, ranging from 2.56 to 2.60. These findings suggest that the biostimulation treatments stabilized soil density to a degree but did not fully restore the mineral density and composition observed in the control samples[13]. The lower specific gravity values in the remediated soils indicate that hydrocarbon contamination and subsequent biodegradation altered the soil matrix, potentially due to the incorporation of lighter organic matter and the loss of denser minerals[52]. This aligns with established studies suggesting that hydrocarbon contamination decreases soil density through organic degradation and mineral dissolution[64].

**Table 9.** Summary of geoenvironmental and geoengineering profiling of the site.

| Parameter | Site Profile | Interpretation & Implications |
|---|---|---|
| TPH Content | 15.17–182.17 mg/kg (variable across depths) | Contaminant affecting soil behaviour |
| Settlement Correlation with TPH | Positive correlation (ranging from 0.25 to 0.95) | Increased compressibility, with BH4 exhibiting stronger effects |
| Coefficient of Consolidation (Cv) vs. TPH | Negative correlation (−0.62 in BH3, minimal in BH4) | Slower consolidation rate in some areas, minor impact in others |
| Specific Gravity vs. TPH | Negative correlation (−0.61 to −0.81) | Hydrocarbons reduce soil density, possibly replacing water in pores |
| Particle Size Distribution (TPH Impact) | Clay: Positive correlation (0.56–0.79), Sand: Negative correlation (−0.54 to −0.82), Gravel: Negative correlation (−0.42 to −0.72) | Contaminated soils exhibit finer particles and fewer coarse fractions |
| Impact Specific Gravity | Ranging from 2.47–2.52 | Lower than control (2.56–2.60), indicating altered soil matrix |
| Soil Classification (Control vs. Impacted) | Control: Poorly Graded Sand with Silt; Remediated: Sandy Lean Clay (> 50% fines) | Hydrocarbon contamination alters soil structure and permeability |
| Water Retention & Permeability | Increased retention, reduced permeability | Higher silt/clay content leads to drainage issues |

**Table 9.** *Cont.*

| Parameter | Site Profile | Interpretation & Implications |
|---|---|---|
| Soil Plasticity and Structural Stability | Increased plasticity | More prone to structural breakdown, erosion risks |
| Hydraulic & Geoenvironmental Effects | Hydrocarbon-induced changes in permeability, creating preferential flow pathways | Potential risks to groundwater and ecosystem stability |
| Soil Nutrient Disruption | Organic acid formation affecting fertility | Lower agricultural viability and reduced microbial activity |
| Consolidation & Compressibility (Impacted) | Settlement: Up to 2.11 mm | Higher than control (1.03 mm), showing residual contamination effects |
| Pre-Consolidation Stress | 128–161 kN/m$^2$ (depth-dependent) | Higher than control (115 kN/m$^2$), indicates altered soil strength and suggests increased resistance to initial compression, however posing concerns to long-term stability |
| Overall Impact on Site Stability | Increased settlement, moderate to slow consolidation | Contamination influences soil properties, requiring targeted remediation strategies |

The particle size distribution analysis demonstrated significant differences between the study and control samples. The impacted soils were predominantly classified as Sandy Lean Clay, with fines exceeding 50%, while the control samples were classified as Poorly Graded Sand with Silt [35]. The higher silt and clay content in the study soils contributed to increased water retention and reduced permeability, which affect soil behaviour under load [52]. Shallower samples, such as SM-1 and SM-4, displayed higher sand content, resulting in better drainage and increased susceptibility to erosion [24]. In contrast, deeper samples, such as SM-3 and SM-6, showed more significant silt and clay fractions, leading to higher water retention and reduced drainage [51]. These variations reflect the differential impacts of hydrocarbon contamination and degradation on soil texture and composition, underscoring the need for targeted interventions based on depth and soil type [52].

The geoenvironmental implications of TPH contamination were significant, influencing soil stability, nutrient dynamics, and water retention capabilities. Hydrocarbon contamination increased soil plasticity, altering the soil structure and making it less resistant to mechanical stress [4]. This was evident in the increased fines content in the remediated soils, which compromised the soil's ability to resist erosion and facilitated the migration of contaminants [13]. The altered permeability in the study soils created conditions conducive to horizontal and vertical contaminant migration, potentially affecting nearby groundwater systems and increasing ecological risks [52]. Studies have shown that hydrocarbons alter soil hydraulic properties, creating preferential flow pathways that can accelerate pollutant spread [65]. This is particularly concerning in regions like Eleme, where groundwater is a critical resource for local communities.

Furthermore, the TPH contamination disrupted the soil's nutrient cycling processes, reducing its capacity to support vegetation [60]. The degradation of hydrocarbons generates organic acids and other byproducts that may temporarily increase soil acidity, further influencing microbial activity and nutrient availability [52]. These changes affect soil fertility, potentially hindering agricultural productivity in impacted areas [51]. The observed higher plasticity in the study soils indicated a greater susceptibility to structural breakdown during wetting and drying cycles, which can exacerbate erosion and reduce the land's agricultural viability [11]. These findings highlight the necessity of integrating soil fertility restoration into remediation strategies to ensure long-term ecological recovery [67]. The alterations in soil composition and hydraulic properties also have broader implications for ecosystem stability. Contaminated soils with reduced permeability and increased fines content are more prone to waterlogging, limiting oxygen availability for plant roots and soil microorganisms [52]. Additionally, hydrocarbons' hydrophobic properties can create impermeable barriers that disrupt water infiltration, further exacerbating drainage issues [4]. These dynamics necessitate careful planning of remediation activities to balance soil restoration with environmental protection.

Consolidation test results further illuminated the geoengineering implications of TPH contamination. Attenuation site soil samples displayed higher compressibility, with settlements of up to 2.11 mm, compared to 1.03 mm in control samples [13]. The increased compressibility was particularly pronounced at shallower depths, where higher TPH concentrations were observed. This finding indicates that

contamination weakens the soil structure by altering void ratios and permeability, making it more susceptible to deformation under load[52]. SM-1 at 0.5 m depth recorded a pre-consolidation stress of 143 kN/m$^2$, while the control sample at the same depth exhibited 115 kN/m$^2$. The differences in consolidation characteristics highlight the ongoing influence of hydrocarbons on soil stability[52]. These results emphasize the importance of integrating environmental and engineering data to evaluate the long-term effectiveness of contaminant degradation and inform engineering designs for attenuated sites[13].

The geoenvironmental assessment underscores the profound impacts of TPH contamination on soil properties, ecosystem stability, and water resource protection. The increased plasticity, reduced permeability, and altered nutrient dynamics observed in the study soils highlight the need for comprehensive, site-specific remediation strategies[52]. These findings collectively contribute to a nuanced understanding of the complex interactions between hydrocarbon impacts, contaminants mass reduction, and soil behaviour, offering valuable guidance for future remediation projects in similar contexts[60].

# 5. Conclusion

This study evaluates the geoenvironmental and geoengineering impacts of hydrocarbon contaminants mass reduction over 6 months at a petroleum-impacted site in Eleme, Rivers State, Nigeria. The research establishes a strong relationship between geophysical resistivity trends and soil properties by integrating Electrical Resistivity Tomography (ERT), Total Petroleum Hydrocarbon (TPH) analysis, and soil mechanical testing. This demonstrates the complementarity of these methods in assessing the attenuation and degradation dynamics of contaminants.

The ERT results delineated subsurface zones with varying resistivity values, closely aligning with hydrocarbon concentrations and soil properties at the borehole locations for the first and second phase sampling and monitoring periods. Boreholes BH1 and BH3, positioned at the 10-meter mark of ERT Lines L1 and L3, exhibited medium resistivity values indicative of sandy-clay soils undergoing moderate biodegradation. Soil samples from these boreholes showed lower TPH concentrations and specific gravity values of 2.51 and 2.52, corresponding to improved drainage and microbial activity that facilitated hydrocarbon degradation. BH2 and BH4, located at the 90-meter mark of Lines L2 and L4, exhibited lower resistivity values at shallow depths, consistent with clay-rich soils retaining higher TPH contaminants biodegradation. These soils demonstrated slightly reduced specific gravity values of 2.47 and 2.49, indicative of finer particles that enhance water retention and support microbial activity but impede drainage. In deeper subsurface zones, ERT imaging revealed higher resistivity values at the 10-meter mark of L1 and L3, correlating with elevated TPH concentrations in BH1 and BH3. At 5.0 m depths, TPH levels reached 182.17 mg/kg and 98.66 mg/kg in these boreholes, reflecting slower biodegradation due to limited oxygen availability. The specific gravity values, averaging 2.48, confirmed reduced soil density influenced by hydrocarbon contamination and mineral dissolution. Conversely, the 90-meter mark of L2 and L4 showed slightly lower resistivity values, aligning with reduced TPH concentrations in the clay-dominated soils of BH2 and BH4 at the same depth. This suggests enhanced biodegradation in these areas, facilitated by nutrient additions and microbial activity for attenuation. Particle size distribution revealed that the study site soils, dominated by silt and clay fractions, exhibited lower permeability and higher water retention, impacting drainage, erosion potential, and contaminant transport. Consolidation tests showed that hydrocarbon contamination increased soil compressibility, with the study samples exhibiting greater settlements under load, emphasizing the weakening of soil structure and its implications for geotechnical stability.

The correlation analysis of TPH content and geotechnical properties shows BH3 has slower consolidation (−0.62 Cv) with moderate settlement increase (0.25), while BH4 exhibits much higher compressibility (0.95) but minimal Cv impact (0.23). TPH strongly reduces specific gravity (more in BH4) and increases clay content while decreasing sand and gravel fractions. Contaminants weaken soil structure, slow drainage, and increase settlement risks, posing geotechnical and environmental concerns. Integrating ERT and soil analysis provides complementary insights into the site's contamination and hydrocarbon attenuation dynamics. The spatial imaging capabilities of ERT identified zones of active biodegradation and mass reduction of less progressive contaminants, which were validated by TPH concentrations

and soil mechanical properties at corresponding borehole locations. Soil analysis further clarified the geophysical patterns observed in the ERT results, illustrating how hydrocarbon contamination affected soil density, permeability, and compressibility. Variations in resistivity across the ERT lines were consistent with changes in soil composition, such as sandy versus clayey soils, and contamination levels, demonstrating ERT's effectiveness in non-invasively characterizing subsurface heterogeneities. The findings highlight the significant progress achieved through biostimulation, with TPH concentrations reduced by 19% to 64% over six months, particularly in shallow subsurface zones where microbial activity was enhanced. However, residual contamination persists in deeper layers, with hydrocarbon concentrations exceeding regulatory limits of the Environmental Guidelines and Standards for the Petroleum Industry in Nigeria (EGASPIN) in some areas and depths, and poses ongoing risks to soil stability and groundwater quality. The study underscores the dynamic interplay between contamination, its mass reduction, and soil properties, revealing the persistent challenges of achieving complete attenuation and the necessity for continued monitoring and tailored interventions.

This research demonstrates the value of integrating ERT and soil chemical and mechanical analyses for adequate site characterization, monitoring, and clean-up planning. The correlations observed between geophysical resistivity patterns, TPH levels, and soil mechanical properties provide a detailed framework for understanding hydrocarbon contamination dynamics and evaluating attenuation progress. While notable improvements in soil quality were observed, the persistence of contamination in deeper zones highlights the need for ongoing monitoring efforts to ensure long-term environmental and geotechnical stability. This approach serves as a model for addressing similar challenges in hydrocarbon-impacted regions worldwide, emphasizing the importance of combining diverse analytical techniques for sustainable land management and environmental restoration. It is therefore recommended that future efforts incorporate extended monitoring durations across seasonal cycles using repeated ERT surveys, groundwater sampling, and geotechnical testing to track long-term attenuation behaviour. The integration of additional geophysical datasets, such as induced polarization (IP), electromagnetic induction (EMI), and soil gas flux measurements, can enhance subsurface discrimination of residual contamination. Furthermore, advanced consolidation testing, suction-controlled triaxial tests, and time-dependent settlement analysis should be applied to assess long-term geotechnical stability under evolving hydrocarbon loads. Investigating deep-layer contamination should include soil coring beyond 6 meters, coupled with vertical electrical sounding (VES) and hydrocarbon fingerprinting to characterize persistent contaminant migration and biodegradation limitations in low-permeability strata.

## Author Contributions

Conceptualization, N.A.O.; methodology, N.A.O.; software, N.A.O.; validation, N.N.N.D., I.A.O., S.I., and S.N.A.R.; formal analysis, N.A.O.; investigation, N.A.O.; resources, N.A.O.; data curation, N.A.O.; writing—original draft preparation, N.A.O.; writing—review and editing, N.N.N.D., I.A.O., S.I., and S.N.A.R.; visualization, N.A.O.; supervision, N.N.N.D., I.A.O., S.I., and S.N.A.R.; project administration, N.A.O., N.N.N.D.; funding acquisition, N.A.O. All authors have read and agreed to the published version of the manuscript.

## Funding

This study was funded by the Petroleum Technology Development Fund (PTDF), Nigeria. (Award No.: PTDF/ED/OSS/PHD/NOA/1714/20).

## Institutional Review Board Statement

Not applicable.

## Informed Consent Statement

Not applicable.

## Data Availability Statement

Data unavailable due to privacy restrictions.

## Acknowledgments

I extend my profound gratitude to the Petroleum Technology Development Fund (PTDF), Nigeria, for funding this

study and the Federal Ministry of Environment, Hydrocarbon Pollution Remediation Project (HYPREP), Nigeria, for providing access to the study site. I also extend sincere appreciation to the management of Petrous Eco Geosolutions, Port Harcourt, Nigeria, for their invaluable support in facilitating this study.

# Conflicts of Interest

The authors declare no conflict of interest.

# References

[1] Ahmed, N.O., Diepiriye, C.O., Chinemerem, P.E., 2019. Geochemical Assessment of Hydrocarbon Contaminated Site in Central Niger Delta, Nigeria. International Journal of Research. 6(6), 505–520.

[2] Eze, S.U., Ogagarue, D.O., Jeong, J., et al., 2025. 4-D ERT Monitoring of Oil Spill Contamination Dynamics and Remediation Planning in Southern Nigeria. Academia Environmental Science and Sustainability. 2(1), 7515. DOI: https://doi.org/10.20935/AcadEnvSci7515

[3] George, S.D., Ahmed, N.O., Yunusa, L.J., et al., 2023. Ecological and Human Health Impacts of Oil Spill-Induced Heavy Metal Contamination in the Niger Delta Environment, Nigeria: Post-Remedial Assessment, Risks, and Mitigation Strategies. International Journal of Ecology and Environmental Science. 5(3), 24–42.

[4] Anyanwu, I.N., Beggel, S., Sikoki, F.D., et al., 2023. Pollution of the Niger Delta with total petroleum hydrocarbons, heavy metals and nutrients in relation to seasonal dynamics. Scientific Reports, 13, 14261. DOI: https://doi.org/10.1038/s41598-023-40995-9

[5] Mohamed, E.S., Jalhoum, M.E.M., Hendawy, E., et al., 2024. Geospatial Evaluation and Bio-Remediation of Heavy Metal-Contaminated Soils in Arid Zones. Frontiers in Environmental Science. 12, 1381409. DOI: https://doi.org/10.3389/fenvs.2024.1381409

[6] Umar, H.A., Khanan, M.F.A., Shiru, M.S., et al., 2023. An Integrated Investigation of Hydrocarbon Pollution in Ahoada Area, Niger Delta Region, Nigeria. Environmental Science and Pollution Research. 30, 116848–116859. DOI: https://doi.org/10.1007/s11356-023-25144-z

[7] Ahmed, N.O., Daud, N.N.N., Okunlola, I.A., 2024b. Geoelectrical Soil Mapping for Subsurface Hydrocarbon Contaminant Characterization and Remediation Site Zoning at Alode, Central Niger Delta, Nigeria. Physics and Chemistry of the Earth. 136(8), 103726. DOI: https://doi.org/10.1016/j.pce.2024.103726

[8] Ehirim, C.N., Adizua, O.F., Okorie, I.P.C., 2016. Geoelectrical Characterization of Matured Petroleum Hydrocarbon Impacted Soil in Port Harcourt, Nigeria. Asian Journal of Earth Sciences. 9, 9–15. DOI: https://doi.org/10.3923/ajes.2016.9.15

[9] Sánchez-Castro, I., Molina, L., Prieto-Fernández, M.-Á., et al., 2023. Past, Present and Future Trends in the Remediation of Heavy-Metal Contaminated Soil: Remediation Techniques Applied in Real Soil-Contamination Events. Heliyon. 9(6), e16692. DOI: https://doi.org/10.1016/j.heliyon.2023.e16692

[10] Ekong, I.S., Nwosu, J.C., 2020. Addressing Hydrocarbon Pollution in Niger Delta Soils Treated with Bioremediation Agents. Journal of Environmental Protection. 7(12), 138672.

[11] Nwankwoala, H.O., Mzaga, T.M., 2017. Geo-Environmental Assessment of Hydrocarbon Contaminated Sites in Parts of Central Swamp Depobelt, Eastern Niger Delta. MOJ Ecology & Environmental Sciences. 2(3), 100–112. DOI: https://doi.org/10.15406/mojes.2017.02.00023

[12] Mekkiyah, H.M., Al-Hamadani, Y.A.J., Abdulhameed, A.A., et al., 2023. Effect of Crude Oil on the Geotechnical Properties of Various Soils and the Developed Remediation Methods. Applied Sciences. 13(16), 9103. DOI: https://doi.org/10.3390/app13169103

[13] Ahmed, N.O., Fagorite, V.I., Chikwado, A.G., et al., 2024a. Pollution Assessment and Index Properties of Okpulor Soils, Rivers State, Nigeria: Geochemical Characterization, Geotechnical and Geoenvironmental Implications. Discover Environment. 2, 60. DOI: https://doi.org/10.1007/s44274-024-00094-6

[14] Ekundayo, E.O., Obuekwe, O., 2000. Effects of an Oil Spill on Soil Physico-Chemical Properties of a Spill Site in a Typic Udipsamment of the Niger Delta Basin of Nigeria. Environmental Monitoring and Assessment. 60, 235–249. DOI: https://doi.org/10.1023/A:1006230025095

[15] Bôto, M.L., Magalhães, C., Perdigão, R., et al., 2021. Harnessing the Potential of Native Microbial Communities for Bioremediation of Oil Spills in the Iberian Peninsula NW Coast. Frontiers in Microbiology. 12, 633659. DOI: https://doi.org/10.3389/fmicb.2021.633659

[16] Fentiman, A., Zabbey, N., 2015. Environmental Degradation and Cultural Erosion in Ogoniland: A Case Study of the Oil Spills in Bodo. The Extractive Industries and Society. 2(4), 615–624. DOI: https://doi.org/10.1016/j.exis.2015.08.006

[17] Eze, S.U., Ogagarue, D.O., Nnorom, S.L., et al., 2021. Integrated Geophysical and Geochemical Methods for Environmental Assessment of Subsurface Hydrocarbon Contamination. Environmental Monitoring and Assessment. 193, 451. DOI: https://doi.org/10.1007/s10661-021-09219-3

[18] Ghrefat, H., Zaman, H., Batayneh, A., et al., 2021. As-

sessment of Heavy Metal Contamination in the Soils of the Gulf of Aqaba (Northwestern Saudi Arabia): Integration of Geochemical, Remote Sensing, GIS, and Statistical Data. Journal of Coastal Research. 37(4), 864–872. DOI: https://doi.org/10.2112/JCOASTRES-D-20-00137.1

[19] Federal Ministry of Environment, 2022. Hydrocarbon Pollution Remediation Project (HYPREP): Report of Hyprep Activities in the Month of December 2021. Available from: https://www.nosdra.gov.ng/wp-content/uploads/2022/02/HYPREP%20JANUARY%20REPORT%202022.pdf (cited 10 May 2025).

[20] United Nations Environment Programme (UNEP), 2011. Environmental Assessment of Ogoniland. Available from: https://ejcj.orfaleacenter.ucsb.edu/wp-content/uploads/2018/03/2011.-UNEP-Report-Environmental-Assessment-of-Ogoniland-2011.pdf (cited 10 May 2025).

[21] Imasuen, O., Galasi, D., Omorogieva, O., 2014. Impact Assessment and Bioremediation of Oil Contaminated Soil: A Case Study of Koko and Ajoki Communities, Niger Delta Nigeria. Journal of Applied Sciences and Environmental Management. 18(1), 55–60. DOI: https://doi.org/10.4314/jasem.v18i1.8

[22] Zabbey, N., Olsson, G.J.G.C., 2017. Conflicts–Oil Exploration and Water. Global Challenges. 1(5), 1600015. DOI: https://doi.org/10.1002/gch2.201600015

[23] Aparicio, J.D., Raimondo, E.E., Saez, J.M., et al., 2022. The Current Approach to Soil Remediation: A Review of Physicochemical and Biological Technologies, and the Potential of Their Strategic Combination. Journal of Environmental Chemical Engineering. 10(2), 107141. DOI: https://doi.org/10.1016/j.jece.2022.107141

[24] Tse, Celestine, A., Eshiemomo, A.U., 2016. Geotechnical Properties of Soils in a Crude Oil Impacted Site in the Niger Delta, Nigeria. IOSR Journal of Applied Geology and Geophysics. 4(2), 69–76.

[25] Opu-Ogulaya, E.D.W., 1973. History of the Creation of the Rivers State of Nigeria: Primer One. Government Printer: Port Harcourt, Nigeria.

[26] Ngofa, O.O., 2006. The Complete History of Eleme. Freedom Press: Ibadan, Nigeria.

[27] Ngulube, I.E., 2011. Orthography of Nigerian Languages Manual X: The Eleme Orthography. Nigerian Educational Research and Development Council (NERDC). Available from: https://www.researchgate.net/publication/280580043 (cited 22 May 2025).

[28] Short, K.C., Stäuble, A.J., 1967. Outline of Geology of Niger Delta. AAPG Bulletin. 51(5), 761–779. DOI: https://doi.org/10.1306/5D25C0CF-16C1-11D7-8645000102C1865D

[29] Akpokodje, E., 1979. The Importance of Engineering Geological Mapping in the Development of the Niger Delta Basin. Bulletin of Engineering Geology and the Environment. 19(1), 101–108. DOI: https://doi.org/10.1007/BF02600459

[30] Amajor, L.C., 1989. Grain Size Characteristics and Geologic Controls on the Bedload Sediments: A Case Study from the Imo River in Southeastern Nigeria. Journal of African Earth Sciences (and the Middle East). 9(3–4), 507–515. DOI: https://doi.org/10.1016/0899-5362(89)90035-3

[31] Reijers, T.J.A., 2011. Stratigraphy and Sedimentology of the Niger Delta. Geologos. 17(3), 133–162. DOI: https://doi.org/10.2478/v10118-011-0008-3

[32] International Atomic Energy Agency (IAEA), 2006. Sampling for Environmental Monitoring. International Atomic Energy Agency: Vienna, Austria.

[33] Loke, M.H., 2004. Tutorial: 2-D and 3-D Electrical Imaging Surveys. Available from: https://www.researchgate.net/profile/Meng-Loke/publication/313653295_Electrical_imaging_surveys_for_environmental_and_engineering_studies/links/61ea69268d338833e38401d6/Electrical-imaging-surveys-for-environmental-and-engineering-studies.pdf (cited 15 May 2025).

[34] Nwilo, P.C., Badejo, O.T., 2006. Impacts and Management of Oil Spill Pollution along the Nigerian Coastal Areas. Administering Marine Spaces: International Issues. 119, 1–15.

[35] ASTM International, 2017. Standard Practice for Classification of Soils for Engineering Purposes (Unified Soil Classification System) (ASTM D2487-17). ASTM International: West Conshohocken, PA, USA. DOI: https://doi.org/10.1520/D2487-17

[36] Lee, H., Sam, K., Coulon, F., et al., 2023. Recent Developments and Prospects of Sustainable Remediation Treatments for Major Contaminants in Soil: A Review. Science of the Total Environment. 168769. DOI: https://doi.org/10.1016/j.scitotenv.2023.168769

[37] Loke, M.H., 2001. Electrical Imaging Surveys for Environmental and Engineering Studies: A Practical Guide to 2D and 3D Surveys (Technical Reports 2000). Universiti Sains Malaysia: Penang, Malaysia.

[38] Aizebeokhai, A.P., 2010. Two-Dimensional and Three-Dimensional Geoelectrical Resistivity Imaging: Theory and Field Design. Scientific Research and Essays. 5(23), 3592–3605.

[39] Ahmed, N.O., Taiwo, O.S., 2023. Spatio-Temporal Analysis of Ilorin Airport on the Land-Use of Ilorin Metropolis, Southwestern Nigeria. Journal of Applied Geospatial Information. 7(2), 948–955. DOI: https://doi.org/10.30871/jagi.v7i2.5693

[40] Loke, M.H., Dahlin, T., 2002. Comparison of the Gauss-Newton and Quasi-Newton Methods in Resistivity Imaging Inversion. Journal of Applied Geophysics. 49(3), 149–162. DOI: https://doi.org/10.1016/S0926-9851(01)00106-9

[41] Loke, M.H., Barker, R.D., 1996. Rapid Least-Squares Inversion of Apparent Resistivity Pseudosections by a Quasi-Newton Method. Geophysical Prospecting. 44, 131–152. DOI: https://doi.org/10.1111/j.1365-2478.1996.tb00142.x

[42] Reynolds, J.M., 1997. An Introduction to Applied and Environmental Geophysics. Wiley: New York, NY, USA.

[43] Che-Alota, V., Atekwana, E.A., Atekwana, E.A., et al., 2009. Temporal Geophysical Signatures Due to Contaminant Mass Reduction. Geophysics. 74(4), B113–B123. DOI: https://doi.org/10.1190/1.3139769

[44] Atekwana, E.A., Sauck, W.A., Aal, G.Z.A., et al., 2002. Geophysical Investigation of Vadose Zone Conductivity Anomalies at a Hydrocarbon Contaminated Site: Implications for the Assessment of Intrinsic Bioremediation. Journal of Environmental Engineering and Geophysics. 7, 103–110. DOI: https://doi.org/10.4133/JEEG7.3.103

[45] Chitea, F., Ioane, D., Kodom, K., 2009. Geoelectrical Evaluation of Soil Properties. In Proceedings of The EGU General Assembly Conference, Vienna, Austria, 19–24 April 2009.

[46] Luan, W., Szelewski, M., 2008. Ultra-Fast Total Petroleum Hydrocarbons (TPH) Analysis with Agilent Low Thermal Mass (LTM) GC and Simultaneous Dual-Tower Injection. Agilent Technologies Application Note: Environmental. 1–8.

[47] Inyang, S.E., Aliyu, A.B., Oyewale, A.O., 2018. Total Petroleum Hydrocarbon Content in Surface Water and Sediment of Qua-Iboe River, Ibeno, Akwa-Ibom State, Nigeria. Journal of Applied Sciences and Environmental Management. 22(12), 1953–1959. DOI: https://doi.org/10.4314/jasem.v22i12.14

[48] Kim, H., Kim, J., Jeong, S., et al., 2019. Method development for the quantitative determination of short-chain fatty acids in microbial culture by GC-FID with SPE cleanup. Journal of Analytical Science and Technology, 10, 36. DOI: https://doi.org/10.1186/s40543-019-0184-2

[49] Department of Petrolm Resources (DPR), 2018. Environmental Guidelines and Standards for the Petroleum Industry in Nigeria (EGASPIN) (Third Edition). Available from: https://pdfcoffee.com/dpr-egaspin-2018-pdf-free.html (cited 15 May 2025).

[50] Awusa, B., 2023. Effect of Hydrocarbon Content on Geotechnical and Chemical Properties of Uyo Coastal Plain Sands, Akwa Ibom State, Eastern Nigeria. Journal of Multidisciplinary Engineering Science and Technology. 8(12), 11885–11891.

[51] Akpan, U.U., Ugwu, D.I., 2019. Geotechnical Effects of Hydrocarbon Contamination in Niger Delta Region of Nigeria. Journal of Geotechnical Engineering. 35(2), 105–119. DOI: https://doi.org/10.1007/s11840-019-00791-1

[52] Akpokodje, O.I., Juwah, H.O., Uguru, H. 2022. Impacts of petroleum spills on geotechnical properties of soils: A review. Journal of Engineering Innovations and Applications, 1(1), 1-6. DOI: https://doi.org/10.31248/JEIA2022.021

[53] American Association of State Highway and Transportation Officials, 2020. AASHTO LRFD Bridge Design Specifications, 9th ed. American Association of State Highway and Transportation Officials: Washington, DC, USA.

[54] Aaltonen, K.J., Osei, E.K., 2022. Electrical Resistivity Tomography in Environmental Monitoring: A Review. Journal of Environmental Science and Technology. 45(8), 1234–1247.

[55] Ovuru, C., Udom, G.J., 2018. Geoelectric Characterization of Recent Hydrocarbon Contaminated Soil and Groundwater in Parts of Ogale Community, Eleme L.G.A. of Rivers State, Nigeria. International Journal of Research. 5(20), 505–514.

[56] Abdullah, W., Aljarallah, R., Alrashidi, A., 2014. Hydrocarbon Oil-Contaminated Soil Assessment Using Electrical Resistivity Topography. Journal of Engineering Research. 2(3), 67–85. DOI: https://doi.org/10.7603/s40632-014-0014-z

[57] Loke, M.H., 2022. Geoelectrical imaging 2D & 3D. Available from: http://www.geotomosoft.com/downloads.php (cited 25 May 2025).

[58] Amadi, E.J., 2016. Application of Electrical Resistivity Method in Groundwater Exploration. SSRN 3505105. DOI: https://doi.org/10.2139/ssrn.3505105

[59] Abdel-Aal, G., Bouazza, A., 2018. Monitoring the Bioremediation of Hydrocarbon-Contaminated Soil Using Electrical Resistivity Tomography. Journal of Applied Geophysics. 154, 245–256.

[60] Raji, L., Obadare, I., Odukoya, A.M., 2017. Geophysical Evaluation of an Oil-Contaminated Coastal Environment, Lagos, Nigeria. Geophysics. 82(6), 5412–5417. DOI: https://doi.org/10.1190/segam2017-17627457.1

[61] Rajendran, S., Priya, T.A.K., Khoo, K.S., et al., 2022. A Critical Review on Various Remediation Approaches for Heavy Metal Contaminants Removal from Contaminated Soils. Chemosphere. 287, 132369. DOI: https://doi.org/10.1016/j.chemosphere.2021.132369

[62] Solomon, L., Ogugbue, C., Okpokwasili, G., 2018. Post-Remediation Assessment of Residual Hydrocarbons in Contaminated Soil in Ogoni Using Gas Chromatographic Fingerprinting Technique and Phytotoxicity Bioassay. Journal of Petroleum & Environmental Biotechnology. 9(2), 367. DOI: https://doi.org/10.4172/2157-7463.1000367

[63] Hanaei, F., Sarmadi, M.S., Rezaee, M., et al., 2021. Experimental Investigation of the Effects of Gas Oil and Benzene on the Geotechnical Properties of Sandy

Soils. Innovative Infrastructure Solutions. 6(2), 61. DOI: https://doi.org/10.1007/s41062-020-00433-5

[64] Rajabi, M., Sharifipour, M., 2019. Geotechnical Properties of Hydrocarbon-Contaminated Soils: A Comprehensive Review. Bulletin of Engineering Geology and the Environment. 78(5), 3685–3717. DOI: https://doi.org/10.1007/s10064-018-1343-1

[65] Adebiyi, F.A., Olatunde, B., 2017. Evaluation of the Effects of Hydrocarbon Contamination on Geotechnical Properties of Soils in the Niger Delta Region of Nigeria. Nigerian Journal of Engineering and Technology. 4(1), 75–84.

[66] Chinwe, A.K., Eze, D.O., 2020. Impact of Petroleum Hydrocarbon Contamination on the Geotechnical Properties of Subsoil: A Case Study of Niger Delta. International Journal of Environmental Science and Technology. 17, 3625–3636. DOI: https://doi.org/10.1007/s13762-020-02934-3

[67] Elisha, A.T., 2012. Effect of Crude Oil Contamination on the Geotechnical Properties of Soft Clay Soils of Niger Delta Region of Nigeria. Electronic Journal of Geotechnical Engineering. 17(M), 1929–1938.

[68] Enemuo, I.O., Nwafor, P.A., 2017. Geotechnical Properties of Crude Oil-Polluted Soils in the Niger Delta, Nigeria. International Journal of Research in Environmental Science. 5(4), 241–256.

[69] Ihejirika, C., Iheanacho, C., Okezie, U., et al., 2019. Post-Remediation Assessment of the Quality of Oil Spill Impacted Soils. Journal of Environmental Pollution Management. 2(2), 203.

[70] Afolabi, O.O., Adesope, O.M., 2022. Ecotoxicological Risk Assessment of Heavy Metals from Remediated Oil Spill Site in Niger Delta Region, Nigeria. Environmental Chemistry and Ecotoxicology. 4, 186–193. DOI: https://doi.org/10.1016/j.enceco.2022.10.001